New Phytologist

Research

# Do stomata optimize turgor-driven growth? A new framework for integrating stomata response with whole-plant hydraulics and carbon balance

**Aaron Potkay**[1,2] and **Xue Feng**[1,2]

[1]Department of Civil, Environmental, and Geo-Engineering, University of Minnesota, Twin Cities, Minneapolis, MN 55455, USA; [2]Saint Anthony Falls Laboratory, University of Minnesota, Twin Cities, Minneapolis, MN 55455, USA

Author for correspondence:
*Aaron Potkay*
*Email: ajpotk@gmail.com*

Received: *24 June 2022*
Accepted: *11 November 2022*

*New Phytologist* (2022)
**doi**: 10.1111/nph.18620

**Key words:** dynamic optimality, nonstructural carbohydrates, source–sink dynamics, stomatal optimization, tree growth, tree hydraulics, turgor-driven expansion.

## Summary

- Every existing optimal stomatal model uses photosynthetic carbon assimilation as a proxy for plant evolutionary fitness. However, assimilation and growth are often decoupled, making assimilation less ideal for representing fitness when optimizing stomatal conductance to water vapor and carbon dioxide. Instead, growth should be considered a closer proxy for fitness.
- We hypothesize stomata have evolved to maximize turgor-driven growth, instead of assimilation, over entire plants' lifetimes, improving their abilities to compete and reproduce. We develop a stomata model that dynamically maximizes whole-stem growth following principles from turgor-driven growth models. Stomata open to assimilate carbohydrates that supply growth and osmotically generate turgor, while stomata close to prevent losses of turgor and growth due to negative water potentials.
- In steady state, the growth optimization model captures realistic stomatal, growth, and carbohydrate responses to environmental cues, reconciles conflicting interpretations within existing stomatal optimization theories, and explains patterns of carbohydrate storage and xylem conductance observed during and after drought.
- Our growth optimization hypothesis introduces a new paradigm for stomatal optimization models, elevates the role of whole-plant carbon use and carbon storage in stomatal functioning, and has the potential to simultaneously predict gross productivity, net productivity, and plant mortality through a single, consistent modeling framework.

## Introduction

Stomata regulate the terrestrial water and carbon cycles through transpiration and photosynthesis (Hetherington & Woodward, 2003), influencing climate through feedback with soil-moisture storage and runoff (Leipprand & Gerten, 2006; Betts *et al.*, 2007), rainfall cycling (Van der Ent & Savenije, 2011; Zemp *et al.*, 2017), atmospheric boundary layer development (Siqueira *et al.*, 2009), atmospheric $CO_2$ concentrations ($c_a$), and air temperatures ($T_a$) (Betts *et al.*, 2000; Cox *et al.*, 2000) among others. Predictions of future climate traditionally employ empirical relationships between stomatal conductance ($g_w$), photosynthetic carbon assimilation ($A_n$), vapor-pressure deficit (VPD; $D_L$), and $c_a$ (e.g. Ball *et al.*, 1987; Leuning, 1995), lacking rigorous plant physiological mechanisms and requiring parameters with little physical meaning. While process-based models of stomatal guard cell dynamics exist (e.g. Buckley *et al.*, 2003, 2012), they remain an open research frontier. Instead, optimization models are replacing empirical formulations for $g_w$ at large scales (Medlyn *et al.*, 2011; De Kauwe *et al.*, 2015; Eller *et al.*, 2020; Sabot *et al.*, 2020). These optimization models are based on the theory that plants have evolved through natural selection to maximize their evolutionary fitness within the limits of genotypic variation and physiological constraints (Mäkelä *et al.*, 2002; Franklin *et al.*, 2020).

Theoretically, optimization models should maximize a plant's reproductive success as the true measure of evolutionary fitness (Mäkelä *et al.*, 2002; Table 1). In practice, however, optimization models for $g_w$ traditionally hypothesize stomata maximize $A_n$ as a proxy for fitness (e.g. Cowan, 1977; Cowan & Farquhar, 1977), which we call assimilation optimization hypotheses (AOHs; see Table 2 for terminology). Maximizing $A_n$ instantaneously would unrealistically predict stomata always maximally open (unless including nonstomatal limitations to photosynthesis). Thus, AOHs introduce additional costs to penalize opening and to predict realistic $g_w$ (Wolf *et al.*, 2016; Wang *et al.*, 2020). These costs and constraints have been associated with water-saving strategies to avoid future water stress (solved either over short durations: Cowan, 1977; Cowan & Farquhar, 1977; Hari *et al.*, 1986; Katul *et al.*, 2010; Medlyn *et al.*, 2011; or dynamically: Cowan, 1982; Mäkelä *et al.*, 1996; Manzoni *et al.*, 2013; Lu *et al.*, 2016; Mrad *et al.*, 2019), xylem embolism (e.g.

**Table 1** Proxies for evolutionary fitness in stomatal optimization.

| Rank (from best to worst) | Plant processes/ proxy for evolutionary fitness | Could this process be satisfactorily modeled at the genesis of stomatal optimization (i.e. Cowan, 1977; Cowan & Farquhar, 1977)? | Can this process be satisfactorily modeled now? | Selected studies of how to model these processes | Selected studies that apply this proxy for fitness to model stomatal conductance |
|---|---|---|---|---|---|
| 1 | Reproduction | × | × | – | – |
| 2 | Growth (*G*) | ×[1] | ✓ | Steppe *et al*. (2006); De Schepper & Steppe (2010); Hölttä *et al*. (2010); Schiestl-Aalto *et al*. (2015); Hayat *et al*. (2017); Cabon *et al*. (2020); Jones *et al*. (2020); Peters *et al*. (2021); Potkay *et al*. (2021a) | Present study |
| 3 | Photosynthetic net carbon assimilation ($A_n$) | ✓ | ✓ | Farquhar *et al*. (1980); Farquhar & Wong (1984); Collatz *et al*. (1991); Evans & Farquhar (1991); De Pury & Farquhar (1997) | Cowan & Farquhar (1977); Cowan (1982); Givnish (1986); Hari *et al*. (1986); Mäkelä *et al*. (1996); Katul *et al*. (2010); Medlyn *et al*. (2011); Manzoni *et al*. (2013); Prentice *et al*. (2014); Lu *et al*. (2016, 2020); Wolf *et al*. (2016); Hölttä *et al*. (2017); Sperry *et al*. (2017); Anderegg *et al*. (2018); Dewar *et al*. (2018, 2022); Eller *et al*. (2018); Bartlett *et al*. (2019); Deans *et al*. (2020); Wang *et al*. (2020) |

A historic inability to satisfactorily mathematically model better proxies of evolutionary fitness, such as plant reproduction and growth, leads to an emphasis on plant processes that could be modeled at the genesis of stomatal optimization, specifically photosynthetic net carbon assimilation. Recent improvements in plant growth modeling may now advance stomatal optimization.

[1]Early work did not consider the role of nonstructural carbohydrate (NSC) storage and thus assumed that an increase in photosynthetic carbon assimilation will always increase growth, which is not necessarily true. Hence, the choice of photosynthetic carbon assimilation as the proxy for fitness was intended to reflect growth optimization.

Wolf *et al*., 2016; Sperry *et al*., 2017), and nonstomatal limitations to photosynthesis (decreased mesophyll conductance and/or photosynthetic capacities; e.g. Givnish, 1986; Dewar *et al*., 2018). Besides nonstomatal limitations (Salmon *et al*., 2020), these costs cannot be measured directly. It is possible to infer them from gas-exchange experiments. However, these experiments are difficult and rarely performed (Hall & Schulze, 1980; Fites & Teskey, 1988; Thomas *et al*., 1999). Overall, AOHs emphasize carbon acquisition, but few AOHs consider how plants actually use carbon once assimilated (Nikinmaa *et al*., 2013; Hölttä *et al*., 2017; Dewar *et al*., 2022). Plant survival, competition, and reproduction should be better reflected by carbon use than by assimilation.

Few AOHs explicitly discuss growth (Givnish & Vermeij, 1976; Cowan, 1982), an important aspect of carbon use. These studies, however, incorrectly assume assimilation and growth are coupled. Assimilation and growth are certainly correlated over annual or longer timescales (Von Allmen *et al*., 2012; Smith & Sperry, 2014) but decoupled over shorter timescales (Cabon *et al*., 2022). Over diurnal timescales, photosynthesis occurs during the day, while most radial growth typically occurs at night or early morning (Peters *et al*., 2021; Zweifel *et al*., 2021). The balance among photosynthesis, growth, and respiration governs the storage of carbon as nonstructural carbohydrates (NSCs), which accumulate during the day (when assimilation exceeds demand) and deplete at night (when demand exceeds assimilation; Smith & Stitt, 2007). Similar NSC patterns occur over seasonal timescales. Trees' NSCs often peak before or at the onset of the growing season (Martínez-Vilalta *et al*., 2016), storing them throughout the winter and sourcing the sprouting of new stems in the following year (Epron *et al*., 2012). In fact, trees store a seeming abundance of NSCs, enough to potentially rebuild their canopies more than four times (Hoch *et al*., 2003). Nonetheless, a consensus on the degree to which growth is limited by NSCs is yet to be reached (Sala *et al*., 2012; Wiley & Helliker, 2012). Are stomatal responses coordinated with growth and NSCs? Could such a potential coordination optimize plants' fitness? AOHs lack a framework to investigate these questions.

We hypothesize stomata have evolved strategies that maximize stem growth over trees' entire lifetimes, which we refer to as the growth optimization hypothesis (GOH). Integrated over time, maximizing growth further maximizes size (height, rooting depth), which directly reflects their abilities to compete for resources (light, water, nutrients; King, 1990; Franklin, 2007). In fact, maximizing height growth is an evolutionarily stable strategy for trees competing for light (Mäkelä, 1985; King, 1990). Size also impacts reproductive success, since most plants reproduce only after achieving a minimum size (Obeso, 2002). Any optimization requires a tradeoff. According to the GOH, stomata open to assimilate carbon to supply growth (i.e. the benefit); however, opening reduces water

**Table 2** Glossary of terminology.

| Term | Meaning |
|---|---|
| Assimilation optimization hypothesis (AOH) | A hypothesis that states that stomata optimize a trade-off between photosynthetic net carbon assimilation ($A_n$) and some additional cost that penalizes excessive stomatal opening |
| Growth optimization hypothesis (GOH) | The hypothesis that stomata optimize turgor-driven growth |
| Growth-optimizing stomata model (GOSM) | A model that predicts the stomatal conductance ($g_c$) that optimizes cambial growth |
| Nonstructural carbohydrates (NSCs) | Large organic macromolecules that provide both the material and energy required for biological chemical reactions, the synthesis of other organic compounds, and the growth of new biomass. Internal plant storage of NSCs buffers the asynchrony of supply and demand over diurnal, seasonal, and decadal timescales and across plant organs |
| NSC-use efficiency (NSCUE) | Cost of depleting NSCs that is associated with the gain of growing new biomass |
| Water-use efficiency (WUE) | Cost of evaporative water loss that is associated with photosynthetic carbon gain |
| Instantaneous optimal solution | Solutions of $g_c$, marginal WUE ($\lambda$), and growth rate ($G$) that optimize growth given prescribed values of the current NSC storage ($C$) and marginal NSCUE ($\eta$) |
| Steady-state optimal solution | Solutions of $g_c$, $\lambda$, $G$, and $C$ that optimize growth once both $C$ and $\eta$ cease changing ($dC/dt = 0$ and $d\eta/dt = 0$) under constant environmental conditions. Steady-state solutions represent the final product of the feedback between $C$ and $\eta$ once they have ceased changing under constant environmental conditions |
| Transient optimal solution | Dynamic solutions of $g_c$, $\lambda$, $G$, and $C$ that optimize growth over a specified duration, which we refer to as the *timescale of optimization*. Transient solutions allow $C$ and $\eta$ to dynamically feedback and evolve in coordination with environmental conditions throughout the timescale of optimization. Environmental conditions may be constant or vary during the timescale of optimization in transient solutions |
| Long-term acclimation of leaf traits to $eCO_2$ | Any solutions under elevated atmospheric $CO_2$ concentrations ($eCO_2$) that reflect leaf-level adaptations to $eCO_2$ that arise slowly over seasonal to annual timescales, including increased leaf areas and reduced photosynthetic capacities. Relevant to Supporting Information Figs S13 and S14 |
| Acclimation to permanent soil water stress | Steady-state optimal solution to permanent soil water stress that reflects a plant's long-term ability to survive and function in different environments of differing soil water availability. Relevant to Figs 4 and 5 |
| Recovery after transient drought stress | Steady-state optimal solution with plentiful soil water and with reduced xylem conductance due to a past transient period of intense soil water stress. This past drought is assumed to have been long enough to reduce xylem conductance while short enough for the simulated plant to still survive. These simulations represent *drought legacy effects* to varying drought intensities. Relevant to Figs 4 and 5 |

potentials ($\psi$) throughout the plant, turgor pressure ($P$) in the cambium and inner bark, and thus growth (i.e. the cost; Figs 1, 2; Sperry *et al.*, 1998; Hölttä *et al.*, 2010). Turgor is an established physiological control on plant growth, including cell expansion (Lockhart, 1965) and division (Kirkham *et al.*, 1972). Turgor also drives the transport of the building blocks of structural biomass (carbohydrates) from where they are produced (leaves) or stored through the phloem to growth sites (Münch, 1930). Additionally, permanent turgor loss leads to mortality of individual cells (i.e. protoplast detachment from the cell wall) and whole plants (through tissue water content loss; Sapes *et al.*, 2019; Preisler *et al.*, 2021; Sapes & Sala, 2021). In fact, an inability to grow often precedes death (Das *et al.*, 2016; Cailleret *et al.*, 2017; DeSoto *et al.*, 2020), potentially due to turgor loss. By maximizing growth and turgor and meristem water content, the GOH reflects a strategy that minimizes desiccation-induced mortality (Supporting Information Notes S1; Section S2).

In this paper, we develop a growth-optimizing stomata model (GOSM) following our GOH that dynamically maximizes the whole-stem growth of an individual tree. We model growth following turgor-driven stem growth models (e.g. Steppe *et al.*, 2006; De Schepper & Steppe, 2010) and source-sink models that consider NSC limitations (e.g. Schiestl-Aalto *et al.*, 2015; Hayat *et al.*, 2017). We compare our GOSM to AOH models as a first-order test. We show the GOH agrees with our current understanding of stomatal regulation to environmental forcing. Finally, we explore our GOH's potential to improve our understanding and ability to predict responses of stomata, growth, and NSC storage, particularly during and after drought.

## Materials and Methods

### Growth-optimizing stomata model

This section summarizes the core assumptions, structure, and key variables of our GOSM (Fig. 1; Table S1). We do not use GOH and GOSM interchangeably. Growth optimization hypothesis refers to a general modeling framework, while GOSM refers to the specific solution to the GOH presented here. Our GOH assumes only that stomata maximize growth, while our GOSM makes many other assumptions to reach a tractable solution. Growth-optimizing stomata model details and assumptions are fully explained in the Supporting Information (Notes S1; Fig. S1), including its limitations (Section S10). The GOH's overarching principle is stomata maximize an individual tree's whole-stem growth over its lifetime. Mathematically, this principle is stated as:

$$\max_{g_c} \int G(C, E)\, dt \qquad \text{Eqn 1}$$

where $g_c$ is the total conductance to $CO_2$, $t$ is time, and $G$ is the whole-tree growth rate expressed in carbon equivalents per unit

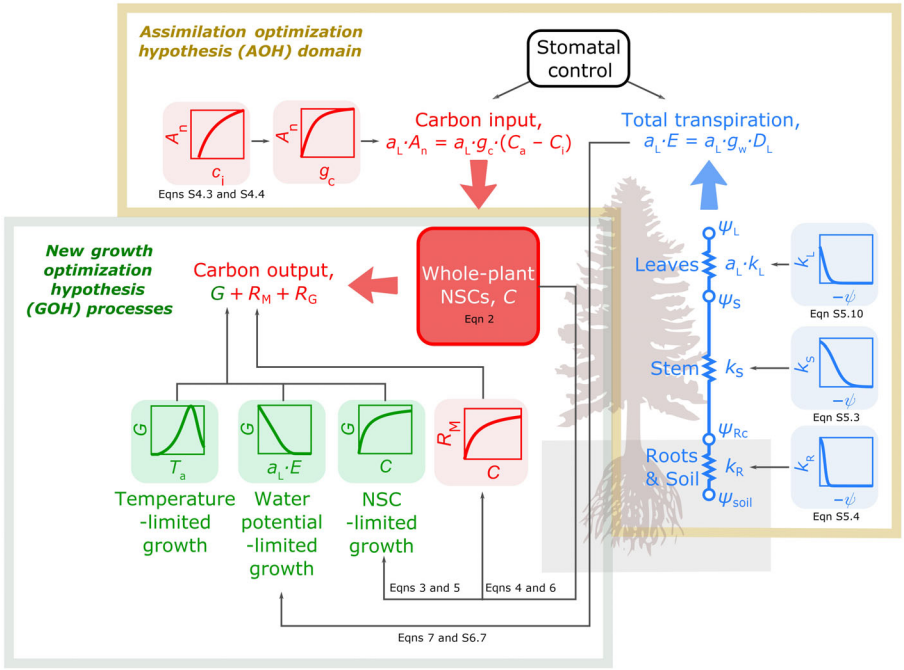


**Fig. 1** Conceptual diagram for our growth-optimizing stomata model (GOSM; see Table S1 for symbols used). Stomata optimize growth by balancing a trade-off between accumulation of nonstructural carbohydrates (NSCs, $C$; red box) and preventing excessively negative water potentials that hamper cell expansion and division. Stomata open to accumulate NSCs through total photosynthetic carbon assimilation ($a_L \cdot A_n$, where $a_L$ is the total leaf area, and $A_n$ is the leaf area-specific carbon assimilation). These NSCs are required to osmotically generate turgor and supply growth ($G$; *NSC-limited growth*), maintenance respiration ($R_M$), and construction respiration ($R_G$, where $R_G \propto G$). NSCs accumulate when carbon inputs ($a_L \cdot A_n$) exceed carbon outputs ($R_M + R_G + G$) and deplete when outputs exceed inputs. In steady state, carbon inputs and outputs are equal, and NSC reserves are stable. Meanwhile, stomata close to prevent cambial water potentials from reaching a threshold, past which growth ceases, by limiting total transpiration ($a_L \cdot E$, where $E$ is the leaf area-specific transpiration; *water potential-limited growth*). The total transpiration is conducted through soil, roots, stems, and then leaves, which are given by their conductances ($k_R$, $k_S$, and $a_L \cdot k_L$, respectively, where $k_R$ is the conductance of the soil and roots in series, and $k_L$ is the leaf conductance per unit leaf area), and soil, root collar xylem, stem apex xylem, and leaf xylem potentials ($\psi_{soil}$, $\psi_{Rc}$, $\psi_S$, and $\psi_L$, respectively). These conductances decline as a result of xylem embolism and loss of soil conductance due to the unsaturation of soil void space (blue subplots on right). Additionally, growth may be limited by cold or hot temperatures (*temperature-limited growth*). Through the diagram, processes are distinguished by color. Red reflects carbon use, blue reflects water use, and green reflects growth, which accounts for both carbon and water use. Thick arrows represent physical fluxes of carbon and water, while thin black arrows represent mathematical relationships between model variables.

time. $G$ depends on other state variables and environmental conditions. The state variables are the leaf area-specific transpiration rate ($E$) and the NSC storage ($C$), while environmental conditions are soil water potential ($\psi_{soil}$), air temperature ($T_a$), the air's relative humidity (RH), and insolation ($I_s$).

We first examine the steady-state GOSM solution to show there exists a $g_c$ that maximizes $G$ (Fig. 2) for the environmental conditions used in Table 3 and later mathematically define the steady-state solution (Eqns 10, 11). Opening stomata releases water vapor as transpiration ($E$), reducing leaf temperature ($T_L$) and leaf-to-air VPD ($D_L$). Opening stomata enables photosynthetic assimilation of $CO_2$ ($A_n$), which depends on $T_L$ by the kinetics of enzymes involved in photosynthesis. Hence, opening stomata *supplies* carbon for growth. Meanwhile, opening 'pulls' xylem sap upward, reducing plant water potentials ($\psi_L$, $\psi_S$, and $\psi_{Rc}$ in Fig. 2), turgor ($P$), and the carbon *demand* for growth ($G_0$ in Fig. 2). As stomata close, *supply* diminishes, while *demand* raises, shrinking carbon storage in the form of NSCs ($C$). Conversely as stomata open, *supply* increases, and *demand* decreases, raising NSCs. In steady state, the actual growth ($G$) balances carbon *supply* with *demand*, and $G$ peaks at an intermediate stomatal aperture ($G_{max}$ in Fig. 2). These $G_0$, $G$, $C$, $A_n$, $E$, $T_L$, $D_L$, $\psi_L$, $\psi_S$, and $\psi_{Rc}$ curves shift as environmental conditions vary, repositioning the optimal $g_c$ (Fig. S2). For example, under soil drought, water potential curves decline, reducing $G_0$ and $G$ curves, elevating the $C$ curve, and shifting $G_{max}$ to a smaller conductance (Fig. S2), thereby changing $g_c$ through changes in *demand* curves. Similarly, elevated atmospheric $CO_2$ concentration shifts $G_{max}$ to a smaller conductance, however, through changes in *supply* curves by elevating $A_n$, $C$, and $G$ curves (Fig. S2). Reducing RH shifts $G_{max}$ to a smaller conductance through changes in the *demand* ($G_0$) curve, particularly by increasing its sensitivity to $g_c$ (larger $|\partial G_0/\partial g_c|$ due to higher VPD). Increasing air temperatures has a small effect on the *supply* ($A_n$) curve; however, changes in *demand* are dominant, closing stomata by increasing the sensitivity of $G_0$ to $g_c$ (i.e. a VPD response) and increasing the maximum value of $G_0$ when stomata are fully closed (a direct growth stimulation by warmer temperatures; Figs S2, S3).

We apply the calculus of variations (Witelski & Bowen, 2015) to solve Eqn 1 for the optimal $g_c$. Several AOH studies have applied the calculus of variations to investigate soil water-saving strategies (Cowan, 1982; Mäkelä *et al.*, 1996; Manzoni *et al.*, 2013;

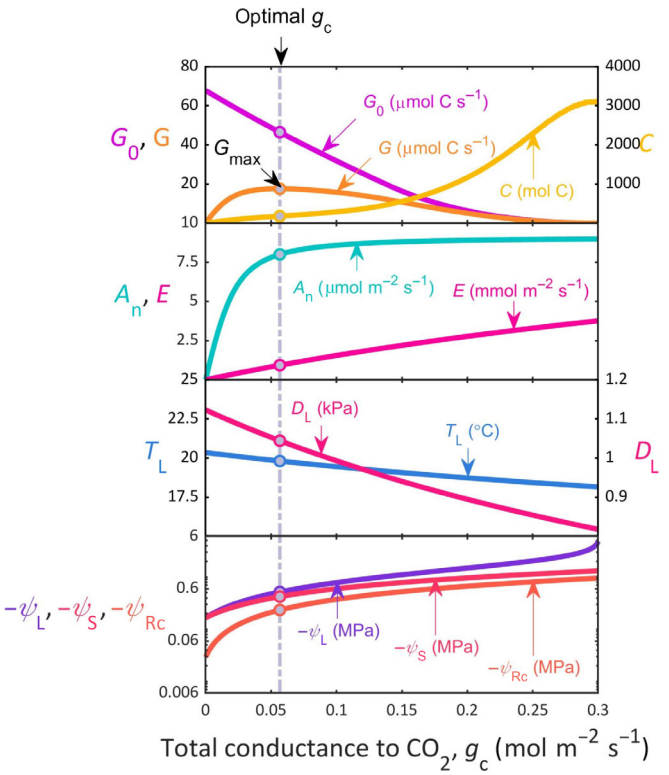


**Fig. 2** Stomatal response model based on the steady-state optimization of turgor-limited growth, showing predictions for photosynthetic $C$ assimilation ($A_n$, teal line), transpiration ($E$, pink line), leaf temperature ($T_L$, blue line), leaf-to-air vapor-pressure deficit (VPD; $D_L$, magenta line), leaf, stem, and root collar water potentials ($-\psi_L$, $-\psi_S$, and $-\psi_{Rc}$, and, dark purple, red, and dark orange lines, respectively), potential growth rate ($G_0$, light purple line), actualized growth rate ($G$, light orange line), and nonstructural carbohydrate (NSC) storage ($C$, yellow line) for potential values of total conductance, $g_c$. Here, we present results from the steady-state version of our model for which both NSC storage and the NSC-use efficiency (NSCUE, $\eta$) are constant ($\dot{C} = 0$ and $\dot{\eta} = 0$) for the environmental conditions and physiological parameters listed in Table 3. The optimal $g_c$ occurs where $G$ is maximum ($G_{max}$, vertical dot-dashed gray line) and coincides with optimal values of $A_n$, $E$, $T_L$, $D_L$, $\psi_L$, $\psi_S$, $\psi_{Rc}$, $G_0$, and $C$ (circles). The upper limit of the $x$-axis ($g_c = 0.3$ mol m$^{-2}$ s$^{-1}$) approximately coincides with the maximum potential $E$, above which $\psi_L$ rapidly approaches negative infinity; thus, the $x$-axis represents the hydraulically viable range of potential $g_c$, which are not prone to runaway embolism.

Mrad *et al.*, 2019). Here, we define whole-plant NSC storage ($C$) as the limiting dynamic resource that trees must conserve to support future growth and respiration. To apply the calculus of variations, we must define the dynamics of $C$:

$$\dot{C} = \frac{\mathrm{d}C}{\mathrm{d}t} = a_L A_n - R_M - R_G - G \qquad \text{Eqn 2}$$

where $a_L$ is the total leaf area, $A_n$ is the leaf area-specific average carbon assimilation rate, $R_M$ is the maintenance respiration of stems and roots, and $R_G$ is the whole-tree growth respiration (Eqns S1.1, S1.2). $A_n$ is modeled following a big-leaf version of the Farquhar *et al.* (1980) model, based on electron transport and carboxylation capacities and their dependence on leaf temperature, the calculation of which considers evaporative leaf cooling (Notes S1; Sections S3, S4). Future GOSM iterations should consider nonstomatal limitations to photosynthesis based on their compatibility with traditional AOH theories (Zhou *et al.*, 2013; Novick *et al.*, 2016).

$R_G$ is proportional to $G$ such that their sum equals $G/(1 - f_c)$, where $f_c$ is a constant less than one, equaling $R_G/(a_L \cdot A_n - R_M)$ when $\dot{C} = 0$ (Eqn S1.6). Both $G$ and $R_M$ are potentially limited by NSCs (Thornley, 1970, 1971; Eqns S1.3, S1.7; $R_G$ may also be NSC-limited, since $R_G \propto G$):

$$G = \sigma_g(C) G_0 \qquad \text{Eqn 3}$$

$$R_M = \sigma_r(C) R_{M,0} \qquad \text{Eqn 4}$$

where $G_0$ and $R_{M,0}$ are maximum potential values of $G$ and $R_M$ if NSCs were nonlimiting, and $\sigma_g$ and $\sigma_r$ are fractions that span between zero (when $C$ is small) and unity (when $C$ is large). We model $\sigma_g$ and $\sigma_r$ similarly to Jones *et al.* (2020) (Eqns S1.4, S1.8):

$$\sigma_g(C) = \frac{C}{C + \gamma_g C_{struct}} \qquad \text{Eqn 5}$$

$$\sigma_r(C) = \frac{C}{C + \gamma_r C_{struct}} \qquad \text{Eqn 6}$$

where $C_{struct}$ is the total dry biomass in carbon equivalents, and $\gamma_g$ and $\gamma_r$ are unitless parameters. We include $C_{struct}$ in Eqns 5 and 6 to signify tree size should influence potential NSC limitations and so $\sigma_g$ and $\sigma_r$ can be related to NSC concentrations rather than whole-tree NSC reserves and are thus presumably less sensitive to tree size. For simplicity, we here model a large, mature tree, enabling us to treat $C_{struct}$ as effectively constant throughout simulations. However, $C_{struct}$ would change dynamically due to $G$ in a full dynamic growth model, especially for young, small trees. This simplification is reasonable if simulations are short or if relative growth rates are small, the latter of which holds for trees that are mature in stature (Valentine & Mäkelä, 2012; Forrester, 2021). Thus, in this study, $\gamma_g \cdot C_{struct}$ and $\gamma_r \cdot C_{struct}$ are more important quantities than $\gamma_g$ and $\gamma_r$, respectively, both of which we indirectly estimated for model performance given our value of $C_{struct}$ (see 'Parameterization' in the Materials and Methods section; Notes S1; Section S8).

$R_{M,0}$ is temperature-dependent and modeled by $Q_{10}$-type equations (Eqn S1.5). $G_0$ is modeled following Potkay *et al.* (2021a), including growth limitations imposed by turgor (Lockhart, 1965; Steppe *et al.*, 2006) and temperature (Parent *et al.*, 2010; Cabon *et al.*, 2020). Their formulation is equivalent to the Lockhart (1965) equation for turgor-driven cell expansion integrated axially along the whole stem within an allometric configuration:

$$G_0 = \tilde{\phi} \frac{C_W}{u_S} \int_0^1 \max(P_0(\tilde{z}) - \Gamma, 0) \mathrm{d}\tilde{z} \qquad \text{Eqn 7}$$

where $\tilde{\phi}$ is an 'effective' whole-tree extensibility that is proportional to the true cell wall extensibility (Potkay *et al.*, 2021a), $C_W$

**Table 3** Default environmental conditions and physiological parameters for our growth-optimizing stomata model (GOSM) and their source.

| Symbol | Value | Units | Meaning | Source |
|---|---|---|---|---|
| Physical constants | | | | |
| $C_p$ | 29.2 | J mol$^{-1}$ K$^{-1}$ | Specific heat capacity of dry air at constant pressure | |
| $g$ | 9.81 | m s$^{-2}$ | Acceleration due to gravity | |
| $R$ | 8.314 | J mol$^{-1}$ K$^{-1}$ | Universal gas constant | |
| $\rho$ | 998 | kg m$^{-3}$ | Density of water | |
| $\sigma$ | $5.67 \times 10^{-8}$ | W m$^{-2}$ K$^{-4}$ | Stefan–Boltzmann constant | |
| Default environmental drivers | | | | |
| $c_a$ | $4.10 \times 10^{-4}$ | mol mol$^{-1}$ | Atmospheric $CO_2$ concentration expressed as a mole fraction | |
| $g_b$ | 2.4 | mol m$^{-2}$ s$^{-1}$ | Boundary layer conductance to vapor | |
| $I_s$ | 600 | W m$^{-2}$ | Incoming solar insolation | |
| $o_a$ | $2.07 \times 10^{-1}$ | mol mol$^{-1}$ | Atmospheric $O_2$ concentration expressed as a mole fraction | |
| $P_{atm}$ | 101.325 | kPa | Atmospheric pressure | |
| RH | 0.4 | – | Atmospheric relative humidity | |
| $T_a$ | 25 | °C | Air temperature | |
| $\Phi$ | 0 | rad | Solar elevation below the zenith | |
| $\psi_{soil}$ | 0 | MPa | Soil water potential | |
| Structural metrics | | | | |
| $a_L$ | 4.9 | m$^2$ | Leaf area | Estimated assuming a leaf area index of 0.4 (LAI = $a_L \cdot \varphi^{-1} \cdot W^{-2}$) based on Scots pine trees at Poblet nature reserve (Prades Mountains, northeast Spain; Poyatos *et al*., 2013); we further assume a ratio of total to projected leaf area, $\varphi$, equal to 3.34 for conical pines (Buckley & Roberts, 2006a) |
| $C_{struct}$ | $1.13 \times 10^3$ | mol C | Whole-tree structural biomass in carbon equivalents | Estimated from $C_W$ assuming a root-to-stem mass ratio of *c*. 0.3 based on Poorter *et al*. (2012) for the given tree size; leaf biomass was estimated assuming a specific leaf area of 0.08 m$^2$ (mol C)$^{-1}$ based on Martínez-Vilalta *et al*. (2009) for Scots pine and that needle dry matter of Scots pine is 50% carbon based on Janssens *et al*. (1999) |
| $C_W$ | $8.3 \times 10^2$ | mol C | Total aboveground stem (wood) biomass in carbon equivalents | Estimated from *H* based on allometric scaling equations with parameters from Potkay *et al*. (2021b) for Scots pine; allometric equation assumes an empirical form factor of 0.5 (Schiestl-Aalto *et al*., 2015) and a stem carbon density of $1.4 \times 10^4$ mol C m$^{-3}$ (Buckley & Roberts, 2006a) |
| $D$ | 9.2 | cm | Diameter at breast height | Estimated from *H* based on allometric scaling equations with parameters from Potkay *et al*. (2021b) for Scots pine; allometric equation is originally based on data from Mencuccini & Grace (1996); Hari & Kulmala (2005); and Reyer *et al*. (2020) |
| $H$ | 14 | m | Stem height | Representative height of Scots pine trees at Poblet nature reserve (Prades Mountains, northeast Spain; Poyatos *et al*., 2013) |
| $W$ | 1.9 | m | Canopy width | Estimated from *H* based on allometric scaling equations with parameters from Potkay *et al*. (2021b) for Scots pine; allometric equation is originally based on data from Pretzsch (2014) |
| $Z$ | 3 | m | Rooting depth | Approximate mean rooting depth for pines from Fan *et al*. (2017) |
| Light interception and photosynthesis | | | | |
| $J_{max,17°C}$ | $1.1 \times 10^{-4}$ | mol m$^{-2}$ s$^{-1}$ | Maximum rate of electron transport at 17°C | Based on Kolari *et al*. (2014) for Scots pine, the temperature dependence of the maximum rate of electron transport, $J_{max}$, is modeled following Harley & Baldocchi (1995) |
| $K_c$ | $2.75 \times 10^{-4}$ | mol mol$^{-1}$ | Michaelis–Menten constant for carboxylation | Hölttä *et al*. (2017) for Scots pine |
| $K_o$ | $4.20 \times 10^{-1}$ | mol mol$^{-1}$ | Michaelis–Menten constant for oxygenation | Hölttä *et al*. (2017) for Scots pine |
| $V_{c,max,17°C}$ | $6.1 \times 10^{-5}$ | mol m$^{-2}$ s$^{-1}$ | Maximum carboxylation rate at 17°C | Based on Kolari *et al*. (2014) for Scots pine, the temperature dependence of the maximum carboxylation rate, $V_{c,max}$, is modeled following Harley & Baldocchi (1995) |

**Table 3** (Continued)

| Symbol | Value | Units | Meaning | Source |
|---|---|---|---|---|
| $\Gamma^*$ | $3.60 \times 10^{-5}$ | mol mol$^{-1}$ | $CO_2$ compensation point | Hölttä *et al*. (2017) for Scots pine |
| $\varepsilon$ | 0.97 | – | Leaf emissivity | Sperry *et al*. (2017) |
| $\theta_c$ | 0.98 | – | Coefficient in hyperbolic minimum of the carboxylation-limited assimilation rate, $A_c$, and the electron transport-limited assimilation rate, $A_j$; $\theta_c A_n^2 - (A_c + A_j) A_n + A_c A_j = 0$ | Sperry *et al*. (2017) |
| $\theta_J$ | 0.90 | – | Coefficient in hyperbolic minimum of maximum electron transport rate, $J_{max}$, and the light-limited rate of electron transport, $J_I$; $\theta_J J^2 - (J_{max} + J_I) J + J_{max} J_I = 0$ | Sperry *et al*. (2017) |
| $\kappa$ | $6.90 \times 10^{-7}$ | mol J$^{-1}$ | Proportionality constant between the light-limited rate of electron transport, $J_I$, and absorbed radiation, $I$; $J_I = \kappa \cdot I$ | Calculated for a quantum yield of 0.3 (mol photon)·(mol e$^-$)$^{-1}$ and an average PAR wavelength of 550 nm |
| $\kappa_L$ | 0.5 | m$^2$ m$^{-2}$ | Canopy light extinction coefficient | Murty *et al*. (1996); Buckley & Roberts (2006a) for lodgepole pine |
| Whole-tree carbon use | | | | |
| $f_c$ | 0.28 | – | Fixed fraction of GPP diverted to growth respiration, $R_G$ | Chung & Barnes (1977) for loblolly pine |
| $R_{M,0,25°C}$ | $5.0 \times 10^{-5}$ | mol C s$^{-1}$ | Maximum stem and root maintenance respiration rate at 25°C | For various combinations of $\gamma_g$ and $\gamma_r$, we calculated $R_{M,0,25°C}$ (Fig. S4), $\widetilde{\phi}_{25°C}$ (Fig. S5), and the steady-state NSC reserve ($\overline{C}$; Fig. S6) that would satisfy two constraints:<br>• the stem and root maintenance respiration rate, $R_M$, equals a target value of $1.5 \times 10^{-5}$ mol C s$^{-1}$ at the default environmental conditions (i.e. values of $c_a$, $I_s$, $o_a$, $P_{atm}$, RH, $T_a$, $\Phi$, and $\psi_{soil}$ from this table)<br>• the net-to-gross primary productivity (NPP : GPP) ratio equals 0.45 (Waring *et al*., 1998; Collalti *et al*., 2020) (NPP : GPP = $G/(R_M + G/(1 - f_c))$) in steady state at the default environmental conditions<br>The target value for $R_M$ was determined given:<br>• a carbon pool-specific root maintenance respiration rate at 15°C, $r_{M,R,15°C}$, equal to $3.1 \times 10^{-8}$ s$^{-1}$ based on Schiestl-Aalto *et al*. (2015) for Scots pine<br>• a temperature dependence for root maintenance respiration following $Q_{10}$ relationship with $Q_{10} = 1.98$ based on Marshall & Waring (1985) for Scots pine<br>• a carbon pool-specific stem maintenance respiration rate at 15°C, $r_{M,W,15°C}$, equal to $6.6 \times 10^{-11}$ s$^{-1}$ based on Schiestl-Aalto *et al*. (2015) for Scots pine<br>• a temperature dependence for stem maintenance respiration following $Q_{10}$ relationship with $Q_{10} = 1.8$ based on Zha *et al*. (2004) for Scots pine<br>• allometric relationships for Scots pine's carbon pools given by Potkay *et al*. (2021b)<br>Given the calculated $\overline{C}$ at ambient and elevated atmospheric $CO_2$ concentrations for various combinations of $\gamma_g$ and $\gamma_r$ (Figs S6, S7), we chose values of $\gamma_g$, $\gamma_r$, and their corresponding $R_{M,0,25°C}$, $\widetilde{\phi}_{25°C}$ values that would satisfy two criteria:<br>• $\overline{C} \approx 175$ mol under ambient atmospheric $CO_2$ concentrations, based on Schiestl-Aalto *et al*. (2019)<br>• the percent increase in $\overline{C}$ due to elevated atmospheric $CO_2$ concentrations was > 0% but did not exceed *c*. 20%, based on Li *et al*. (2018) |

**Table 3** (Continued)

| Symbol | Value | Units | Meaning | Source |
|---|---|---|---|---|
| $\gamma_g$ | 0.26 | – | Shape parameter for $\sigma_g$, the NSC substrate limitation function for whole-tree growth, $G$ | |
| $\gamma_r$ | 0.38 | – | Shape parameter for $\sigma_r$, the NSC substrate limitation function for stem and root maintenance respiration, $R_M$ | |
| Turgor-limited growth | | | | |
| $c_{m,1}$ | 0.48 | mol kg$^{-1}$ | Intercept of the empirical relationship between phloem sap molality, $m_p$, and stem water potential, $\psi_S$ ($m_p = c_{m,1} - c_{m,2} \cdot \psi_S$) | Paljakka *et al*. (2017) for Scots pine |
| $c_{m,2}$ | 0.13 | mol kg$^{-1}$ MPa$^{-1}$ | Slope (negative) of the empirical relationship between phloem sap molality, $m_p$, and stem water potential, $\psi_S$ ($m_p = c_{m,1} - c_{m,2} \cdot \psi_S$) | Paljakka *et al*. (2017) for Scots pine |
| $c_{\Pi,1}$ | 0.998 | – | Linear coefficient between osmotic potential, $\pi$, and phloem sap molality, $m_p$ | ($\pi = -\overline{\omega} \cdot \rho \cdot R \cdot T_a \cdot \left(c_{\Pi,1} \cdot m_p + c_{\Pi,2} \cdot m_p^2\right)$, where $\overline{\omega} = 10^{-6}$ MPa Pa$^{-1}$) |
| | | Michel (1972); Thompson & Holbrook (2003a) for sucrose | | |
| $c_{\Pi,2}$ | 0.089 | kg mol$^{-1}$ | Quadratic coefficient between osmotic potential, $\pi$, and phloem sap molality, $m_p$ | ($\pi = -\overline{\omega} \cdot \rho \cdot R \cdot T_a \cdot \left(c_{\Pi,1} \cdot m_p + c_{\Pi,2} \cdot m_p^2\right)$, where $\overline{\omega} = 10^{-6}$ MPa Pa$^{-1}$) |
| | | Michel (1972); Thompson & Holbrook (2003a) for sucrose | | |
| $u_S$ | 0.25 | – | Fraction of new growth allocated to stems | Xia *et al*. (2019); Potkay *et al*. (2021b) for mature tree |
| $\Gamma$ | 0.75 | MPa | Threshold that turgor, $P$, must exceed for stem expansion | Potkay *et al*. (2021a) |
| $\widetilde{\phi}_{25°C}$ | $4.6 \times 10^{-8}$ | MPa$^{-1}$ s$^{-1}$ | Effective whole-tree extensibility at 25°C | See the Source section in this table for $R_{M,0,25°C}$, $\gamma_g$, and $\gamma_r$ parameters. The temperature dependence of the effective whole-tree extensibility, $\widetilde{\phi}$, is modeled following an equation similar to Johnson *et al*. (1942) and Parent *et al*. (2010) using the parameters reported by Cabon *et al*. (2020) and Peters *et al*. (2021). Unlike Johnson *et al*. (1942) and Parent *et al*. (2010), $\widetilde{\phi}$ here continuously approaches zero as temperatures approach 5°C, the growth threshold suggested by Körner (2008) (Fig. S3) |
| Xylem hydraulics | | | | |
| $k_L$ | $1.6 \times 10^{-2}$ | mol $H_2O$ m$^{-2}$ s$^{-1}$ MPa$^{-1}$ | Maximum leaf xylem conductance per leaf area | Buckley & Roberts (2006a) for loblolly pine |

**Table 3** (Continued)

| Symbol | Value | Units | Meaning | Source |
|---|---|---|---|---|
| $k_R$ | $2.30 \times 10^{-2}$ | mol $s^{-1}$ $MPa^{-1}$ | Maximum soil-root conductance | Estimated given the values of $H$, $Z$, and $a_L$ from this table ($H$ and $a_L$ are based on Poyatos *et al*., 2013) assuming:<br>• belowground resistance is 45% of total resistance based on Martínez-Vilalta *et al*. (2007) for Scots pine<br>• a midday leaf area-specific transpiration, $E$, equal to $1.6 \times 10^{-3}$ mol $m^{-2}$ $s^{-1}$ coincides with pre-dawn and midday leaf water potentials, $\psi_{pd}$ and $\psi_{md}$, equal to −0.72 and −1.50 MPa, respectively, based on Poyatos *et al*. (2013)<br>• roots operate at 80% of their maximum conductance based on Lintunen *et al*. (2020) for Scots pine |
| $k_S$ | $9.76 \times 10^{-2}$ | mol $s^{-1}$ $MPa^{-1}$ | Maximum whole-stem xylem conductance | Estimated from $H$ based on allometric scaling equations with parameters from Potkay *et al*. (2021b) for Scots pine; allometric equation is originally based on data from Mencuccini & Grace (1996) and Hölttä *et al*. (2013); we further assumed in this calculation that the sapwood fraction of the total wood is 94% for Scots pine based on Mencuccini & Grace (1996) |
| $\alpha_L$ | 1.5 | $MPa^{-1}$ | Shape parameter for describing the loss of leaf conductance under increasingly negative water potentials | Estimated by fitting exponential sigmoidal curves to needle conductance measurements by Domec *et al*. (2009) for loblolly pine |
| $\alpha_R$ | 3.5 | $MPa^{-1}$ | Shape parameter for describing the loss of belowground conductance under increasingly negative water potentials | Estimated by fitting exponential sigmoidal curves to belowground conductance measurements by Poyatos *et al*. (2018) for Scots pine |
| $\alpha_S$ | 0.8 | $MPa^{-1}$ | Shape parameter for describing the loss of stem conductance under increasingly negative water potentials | Estimated by fitting exponential sigmoidal curves to branch conductance measurements by Torres-Ruiz *et al*. (2016) for Scots pine |
| $\beta_L$ | −0.75 | MPa | Water potential at which half of the leaf conductance is lost (i.e. P50 for leaves) | Estimated by fitting exponential sigmoidal curves to needle conductance measurements by Domec *et al*. (2009) for loblolly pine |
| $\beta_R$ | −1.1 | MPa | Water potential at which half of the belowground conductance is lost (i.e. P50 for the root-soil system) | Estimated by fitting exponential sigmoidal curves to belowground conductance measurements by Poyatos *et al*. (2018) for Scots pine |
| $\beta_S$ | −3.3 | MPa | Water potential at which half of the stem conductance is lost (i.e. P50 for stems) | Estimated by fitting exponential sigmoidal curves to branch conductance measurements by Torres-Ruiz *et al*. (2016) for Scots pine |
| Parameters for other models | | | | |
| $\mu_w$ | $1 \times 10^{-3}$ | mol $mol^{-1}$ | Constant marginal carbon cost of water; used in the Cowan & Farquhar (1977) model | Chosen to agree with the other models under the default environmental conditions |
| $\beta$ | 145 | – | Ratio of costs associated with carboxylation capacity, $V_{c,max}$, and transpiration, $E$; used in the Prentice *et al*. (2014) model | Smith *et al*. (2019); Lavergne *et al*. (2020b) |
| $\beta_1$ | $4 \times 10^{-6}$ | mol $m^{-2}$ $s^{-1}$ $MPa^{-2}$ | Quadratic coefficient between hydraulic risk, Θ, and leaf water potential, $\psi_L$; used in the Anderegg *et al*. (2018) model; $\Theta = \beta_1 \cdot \psi_L^2 + \beta_2 \cdot \psi_L + \beta_3$ | Zenes *et al*. (2020) for Ponderosa pine |

**Table 3** (Continued)

| Symbol | Value | Units | Meaning | Source |
|---|---|---|---|---|
| $\beta_2$ | 0 | mol m$^{-2}$ s$^{-1}$ MPa$^{-1}$ | Linear coefficient between hydraulic risk, $\Theta$, and leaf water potential, $\psi_L$; used in the Anderegg *et al.* (2018) model; $\Theta = \beta_1 \cdot \psi_L^2 + \beta_2 \cdot \psi_L + \beta_3$ | Set to zero since Zenes *et al.* (2020) found that $\beta_1$ and $\beta_2$ covaried |
| $\beta_3$ | 0 | mol m$^{-2}$ s$^{-1}$ | Minimum hydraulic risk, $\Theta$, used in the Anderegg *et al.* (2018) model; $\Theta = \beta_1 \cdot \psi_L^2 + \beta_2 \cdot \psi_L + \beta_3$ | Set to zero to compare with other models, all of which have zero hydraulic risk at their maximum leaf water potentials and minimum transpiration rates |
| $\psi_{L,crit}$ | −2 | MPa | Critical leaf water potential, $\psi_L$, at which the carboxylation capacity, $V_{c,max}$, equals zero; used in the Dewar *et al.* (2018) model | Dewar *et al.* (2018) |

is the stem biomass in carbon equivalents, $\tilde{z}$ is the axial distance along the stem from the stem apex normalized by the tree height, $P_0$ is axially variable potential turgor if NSCs were not limiting, which may exceed the true turgor limited by NSCs, $P$, and $\Gamma$ is the threshold turgor must exceed before growth occurs (Eqn S6.1). Hence, $G_0$ depends on the average of $\max(P_0(z)-\Gamma, 0)$ over the tree height between the stem apex ($\tilde{z} = 0$) and the root collar ($\tilde{z} = 1$). We model the temperature dependence of $\tilde{\phi}$ following Parent *et al.* (2010) using parameters provided by Cabon *et al.* (2020) and Peters *et al.* (2021) (Fig. S3). Our approach to estimate $P_0$ (Notes S1; Section S6) and its limitations and future improvements (Notes S1; Sections S10.1, S10.2) are discussed in the Supporting Information.

Upon applying the calculus of variations (Witelski & Bowen, 2015) to solve Eqn 1 for the $g_c$ that maximizes growth (Notes S1; Section S2), the solution is defined in terms of the *marginal carbon cost of water*, $\chi_w$. When stomata behave optimally, $\chi_w$ equals the *marginal carbon profit of water*, $dA_n/dE$, which we denote by $\lambda$ as shorthand based on similar usage in *Gain-Risk* AOHs (Wolf *et al.*, 2016; Wang *et al.*, 2020; Figs 3a,b, S1), for which an alternate expression can be independently formulated from photosynthesis and gas exchange following Buckley *et al.* (2002, 2017) (Eqn S4.11). Simply, when water is more costly (larger $\chi_w$), stomata close (smaller $g_c$). The same principle may be expressed in terms of hydraulic cost, $\Theta = \int \chi_w \, dE$, through which *Gain-Risk* AOHs are often framed (Wang *et al.*, 2020; Fig. 3c,d; Eqn S2.5). That is, stomata close as $\Theta$ increases. The GOH solution for $\chi_w$ is:

$$\chi_w \equiv \left(\frac{1}{1-f_c} - \frac{1}{\eta}\right)\frac{1}{a_L}\frac{\partial G}{\partial E} = \left(\frac{1}{\eta} - \frac{1}{1-f_c}\right)\frac{1}{a_L}\left|\frac{\partial G}{\partial E}\right| \quad \text{Eqn 8(a)}$$

$$\chi_w \equiv \left(\frac{1}{1-f_c} - \frac{1}{\eta}\right)\frac{\sigma_g}{a_L}\frac{\partial G_0}{\partial E} = \left(\frac{1}{\eta} - \frac{1}{1-f_c}\right)\frac{\sigma_g}{a_L}\left|\frac{\partial G_0}{\partial E}\right| \quad \text{Eqn 8(b)}$$

$$\chi_w = \lambda \quad \text{Eqn 8(c)}$$

We list the identity of $\chi_w$ twice to distinguish between a general identity (Eqn 8a) and an identity specific to how we model $G$ here (Eqn 8b). Importantly, Eqn 8(a) holds for any growth-optimizing framework regardless of how growth is modeled (as long as $G$ can be formulated as a function of $E$), while Eqn 8(b) is particular to our current GOSM. $\partial G_0/\partial E$ in Eqn 8(b) is solved by differentiating Eqn 7 with respect to $E$ (Eqns S6.7, S6.11; $\partial G_0/\partial E \leq 0$). We informally refer to the solution of the Lagrange multiplier, $\eta$, as the marginal NSC-use efficiency (NSCUE; Notes S1; Section S2) ($0 \leq \eta < 1 - f_c$), which is analogous to the inverse of the *marginal carbon cost of carbon use* (Buckley & Roberts, 2006b) and represents the cost of spending NSCs on growth and respiration. Large $\eta$ describes a strategy in which NSCs are highly valued, in which stomata open (small $\chi_w$; large $g_c$; Fig. 3a) to increase $A_n$, decrease $G$, and maintain or even elevate NSCs. When $\eta$ is small, NSCs are 'cheap', prompting plants to spend their NSCs by closing stomata (large $\chi_w$ and $\Theta$; small $g_c$; Fig. 3a,c) to increase $G$. Fig. 3(a) shows potential

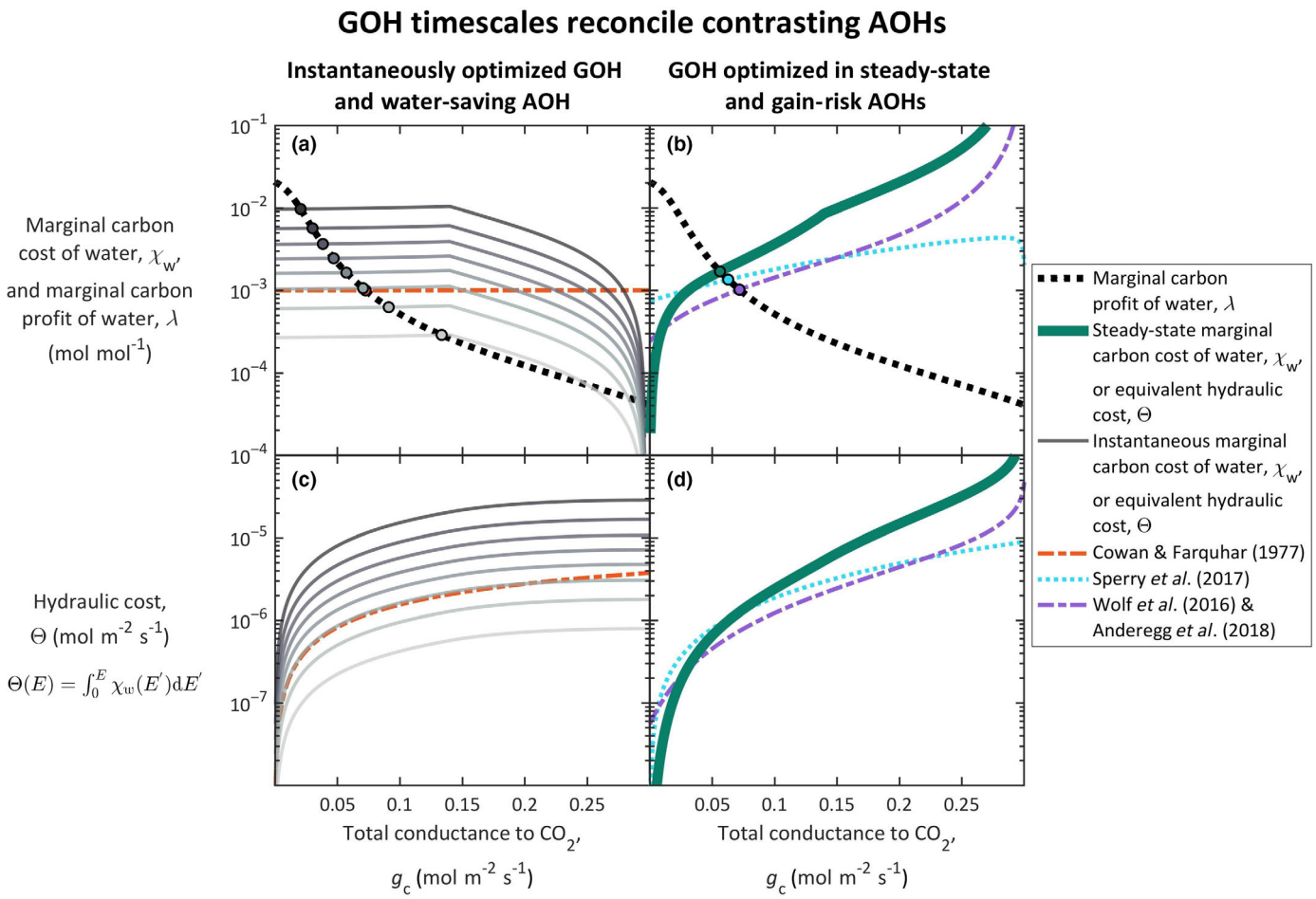


**Fig. 3** Marginal carbon profit and cost ($\lambda$ and $\chi_w$) (a, b) as well as hydraulic cost ($\Theta$, where $d\Theta/dE = \chi_w$; Wolf *et al.*, 2016) (c, d) predicted by the growth optimization hypothesis (GOH) and several assimilation optimization hypotheses (AOHs) for potential values of total conductance values, $g_c$, for the environmental conditions and physiological parameters listed in Table 3. (a) Instantaneous marginal costs, $\chi_w$, calculated for different NSCUEs ($\eta$) according to the GOH, with $\eta$ ranging from 20% to 90% of its maximum value ($1 - f_c$) in 10% increments (darkest to lightest). Instantaneous $\chi_w$ was calculated for an NSC storage based on measurements of Scots pine of similar size as our simulated tree by Schiestl-Aalto *et al.* (2019) ($C = 175$ mol). In (a), note that $\chi_w = 0$ for $g_c > c.$ 0.3 mol m$^{-2}$ s$^{-1}$ (coinciding with where there is no growth), regardless of $\eta$. (b) Steady-state marginal cost, $\chi_w$, calculated when both NSC storage and NSCUE have reached constant state ($\dot{C} = 0$ and $\dot{\eta} = 0$) according to the GOH. Intersection of $\lambda$ and $\chi_w$ or $\overline{\chi}_w$ curves (circles in a and b) coincides with the optimal $g_c$. When multiple intersections occur for instantaneous optimizations in (a), we select the lesser $g_c$, which coincides with higher growth rates; the greater $g_c$ typically coincides with insignificant growth. (c) Hydraulic cost from instantaneous GOH corresponding to (a). (d) Hydraulic cost from steady-state GOH corresponding to (b).

$\chi_w$ and $\lambda$ calculated across potential $g_c$ for a range of $\eta$ using the environmental conditions and physiological parameters listed in Table 3. The $\chi_w$ and $\lambda$ curves intersect at the optimal $g_c$ (circles in Fig. 3a). Indeed, the optimal $g_c$ increases as $\eta$ increases. In the range of $g_c$ values that $\chi_w$ and $\lambda$ typically intersect, $\chi_w$ is near constant due to near-constant $\partial G_0/\partial E$. At larger $g_c$, $\chi_w$ declines to zero as $E$ increases, $\psi$ becomes more negative, turgor declines, and $G_0$, $\partial G_0/\partial E$, and $\chi_w$ all approach zero. Hence, multiple intersection points may exist in the instantaneous optimization. In this case, we select the lesser $g_c$, which coincides with the higher $G$, since greater $g_c$ reduces $G$ (Notes S1; Section S2).

The calculus of variations suggests $\eta$ is not constant and changes dynamically in response to environmental conditions, carbon use, and NSC storage (Eqn S2.6):

$$\dot{\eta} = \frac{d\eta}{dt} = \eta\frac{\partial R_M}{\partial C} + \left(\frac{\eta}{1-f_c} - 1\right)\frac{\partial G}{\partial C} = \eta\frac{\partial \sigma_r}{\partial C}R_{M,0} + \left(\frac{\eta}{1-f_c} - 1\right)\frac{\partial \sigma_g}{\partial C}G_0 \quad \text{Eqn 9}$$

According to Eqn 9, $\partial R_M/\partial C > 0$. This is because we do not expect excess NSCs to penalize growth (i.e. $\partial G/\partial C \geq 0$), and $0 \leq \eta < 1 - f_c$, which means that $\eta$ would eventually become negative (i.e. $\dot{\eta} < 0$ for all times) if maintenance respiration either were independent of NSCs ($\partial R_M/\partial C = 0$) or declined under elevated NSC storage ($\partial R_M/\partial C < 0$). However, $\eta$ must be non-negative. Thus, the existence of an optimal solution requires $\partial R_M/\partial C > 0$, which indeed has empirical support (Sevanto *et al.*, 2014; Collins *et al.*, 2021) and thus justifies the functional forms of Eqns 4 and 6.

To test our GOH under varied environmental conditions, we consider solutions in steady state when carbon assimilation and use are in balance ($\dot{C} = 0$) and the marginal NSCUE has ceased changing ($\dot{\eta} = 0$). Steady state is only an approximation of how plants behave in reality; nonetheless, it provides insights into the optimal stomatal behavior to environmental cues. Unlike instantaneous solutions, it reflects stomata responses after they have equilibrated to environmental variations if those conditions were sustained constantly over an extended period of time (Feng *et al.*, 2015). We denote steady-state values by symbols with a vinculum (e.g. $\overline{\eta}$, $\overline{C}$). Setting Eqn 9 to zero and rearranging gives the steady-state marginal NSCUE (Eqn S2.7):

$$\overline{\eta} = \left(1-f_c\right)\frac{\frac{\partial \overline{G}}{\partial \overline{C}}}{\frac{\partial \overline{G}}{\partial \overline{C}} + \left(1-f_c\right)\frac{\partial \overline{R}_M}{\partial \overline{C}}} = \left(1-f_c\right)\frac{\frac{\partial \overline{\sigma}_g}{\partial \overline{C}}\overline{G}_0}{\frac{\partial \overline{\sigma}_g}{\partial \overline{C}}\overline{G}_0 + \left(1-f_c\right)\frac{\partial \overline{\sigma}_r}{\partial \overline{C}}R_{M,0}} \qquad \text{Eqn 10}$$

Setting Eqns 8 and 10 equal and rearranging defines the steady-state *marginal cost of water* (Eqn S2.8).

$$\overline{\chi}_w = -\frac{1}{a_L}\frac{\partial \overline{G}}{\partial \overline{E}}\frac{\frac{\partial \overline{R}_M}{\partial \overline{C}}}{\frac{\partial \overline{G}}{\partial \overline{C}}} = -\frac{\overline{\sigma}_g}{a_L}\frac{\partial \overline{G}_0}{\partial \overline{E}}\frac{R_{M,0}}{\overline{G}_0}\frac{\frac{\partial \overline{\sigma}_r}{\partial \overline{C}}}{\frac{\partial \overline{\sigma}_g}{\partial \overline{C}}} = \frac{\overline{\sigma}_g}{a_L}\left|\frac{\partial \overline{G}_0}{\partial \overline{E}}\right|\frac{R_{M,0}}{\overline{G}_0}\frac{\frac{\partial \overline{\sigma}_r}{\partial \overline{C}}}{\frac{\partial \overline{\sigma}_g}{\partial \overline{C}}} \qquad \text{Eqn 11}$$

Contrary to the instantaneous solution, the steady-state solution given by Eqn 11 has mathematically unique solution with a single $g_c$ at which $\lambda = \overline{\chi}_w$ (Fig. 3b). This uniqueness results from $\overline{\chi}_w$ being a positive, increasing function of $g_c$ and from $\overline{\chi}_w < \lambda$ at $g_c = 0$ (Wang *et al.*, 2020). In fact, $\overline{\chi}_w$ must equal zero at $g_c = 0$ due to the $\overline{\sigma}_g$ term in Eqn 11, which equals zero when $g_c = 0$ resulting from insignificant NSC storage and carbon *supply* limitations (Fig. 2). $\overline{\chi}_w$ is an increasing function of $g_c$, because of the $\overline{G}_0$ term in the denominator of Eqn 11, which approaches zero faster than the decline in the other terms in the numerator.

## Parameterization

We parameterized our GOSM with values reported or estimated from the existing literature to represent an evergreen conifer, many of which were synthesized by Potkay *et al.* (2021b) (Table 3). The majority of the parameters originate from studies of Scots pine (*Pinus sylvestris*); however, several parameters represent loblolly pine (*Pinus taeda*). No parameters were finely tuned to match observations, and we focus on the model's ability to capture fundamental stomatal responses by using parameters that are as physically based as possible. Four parameters were estimated indirectly ($R_{M,0}$, $\widetilde{\phi}$, $\gamma_g$, and $\gamma_r$) to satisfy a net-to-gross primary productivity ratio of 0.45 (Waring *et al.*, 1998; Collalti *et al.*, 2020) and realistic NSC reserves under ambient and elevated $c_a$ (Figs S4–S7; Notes S1; Section S8).

## Responses to the environment

To test our GOSM to environmental cues, we consider both instantaneous and steady-state solutions. We determine instantaneous solutions for known $\eta$ and $C$ (Fig. 4; Eqn 10), assuming an NSC storage based on measurements of Scots pine of similar size as our simulated tree by Schiestl-Aalto *et al.* (2019) ($C$ = 175 mol). Steady-state solutions require no assumptions about $\overline{\eta}$ or $\overline{C}$. Their values emerge from the optimization (Eqns 10, 11). We test GOSM predictions to VPD (by varying atmospheric relative humidity, RH; 0.1–0.8), soil water potential ($\psi_{soil}$; −0.8 to 0 MPa), atmospheric $CO_2$ concentration ($c_a$; 250–650 ppm), and the loss of hydraulic conductance due to past drought. We quantify past drought severity by the minimum experienced soil water potential causing conductance loss ($\psi_{soil}^{min}$; −2.4 to −0.02 MPa) and present results from two approaches for conductance hysteresis (Notes S1; Section S9). One hysteresis approach considers the true loss of conductance (e.g. Mackay *et al.*, 2015), and the alternative approach postulates plants maintain the optimal $\psi_L$ as if embolism were impermanent (Venturas *et al.*, 2018). We hold the other environmental conditions constant at the default values listed in Table 3. We consider how the environmental cues influence total conductance ($g_c$), the marginal WUE ($\lambda$), growth ($G$), and NSC storage ($C$).

Furthermore, we consider the possibility of long-term acclimation of leaf traits (leaf area, $a_L$, and photosynthetic capacities) to elevated $c_a$ ($eCO_2$) when testing our GOSM to increased $c_a$. In acclimated simulations, we increased $a_L$ by a factor of 1.25 based on Lauriks *et al.* (2021), reduced the maximum carboxylation capacity ($V_{c,max}$) by a factor of 0.90, and reduced the maximum electron transport capacity ($J_{max}$) by a factor of 0.95 based on Ainsworth & Rogers (2007).

Crucially, instantaneous optimization solutions may be neither realistic nor meaningful. There exists a temporal mismatch between key model variables required to solve the instantaneous optimization ($\eta$, $C$) and environmental conditions, since instantaneous optimizations do not consider their key feedback (Eqn 11). Instantaneous results are appropriate when stomatal responses due solely to environmental conditions (i.e. at constant $\eta$ and $C$) are far faster than those due to dynamics in $\eta$ and $C$ that arise from environmental changes. These scenarios apply when testing environmental factors that vary significantly over hourly or shorter timescales in real environments (e.g. $D_L$) but are inappropriate for more slowly changing factors (e.g. $\psi_{soil}$, $\psi_{soil}^{min}$, and $c_a$). Our steady-state results, nevertheless, capture the key feedback that ensures realistic responses of $\eta$, $C$, and $g_c$ for slowly changing conditions, because steady-state predictions represent responses that have equilibrated to environmental conditions.

Additionally, we compare steady-state solutions to predictions by several extensively tested AOH models (Table S2), including those by Cowan & Farquhar (1977), Prentice *et al.* (2014), Wolf *et al.* (2016), Anderegg *et al.* (2018), Sperry *et al.* (2017), Eller *et al.* (2018), Dewar *et al.* (2018), and Wang *et al.* (2020). This comparison provides a first-order, quantitative test for the GOSM's predicted $g_c$, while previous tests checked for realistic qualitative trends. The comparison also assesses whether GOH

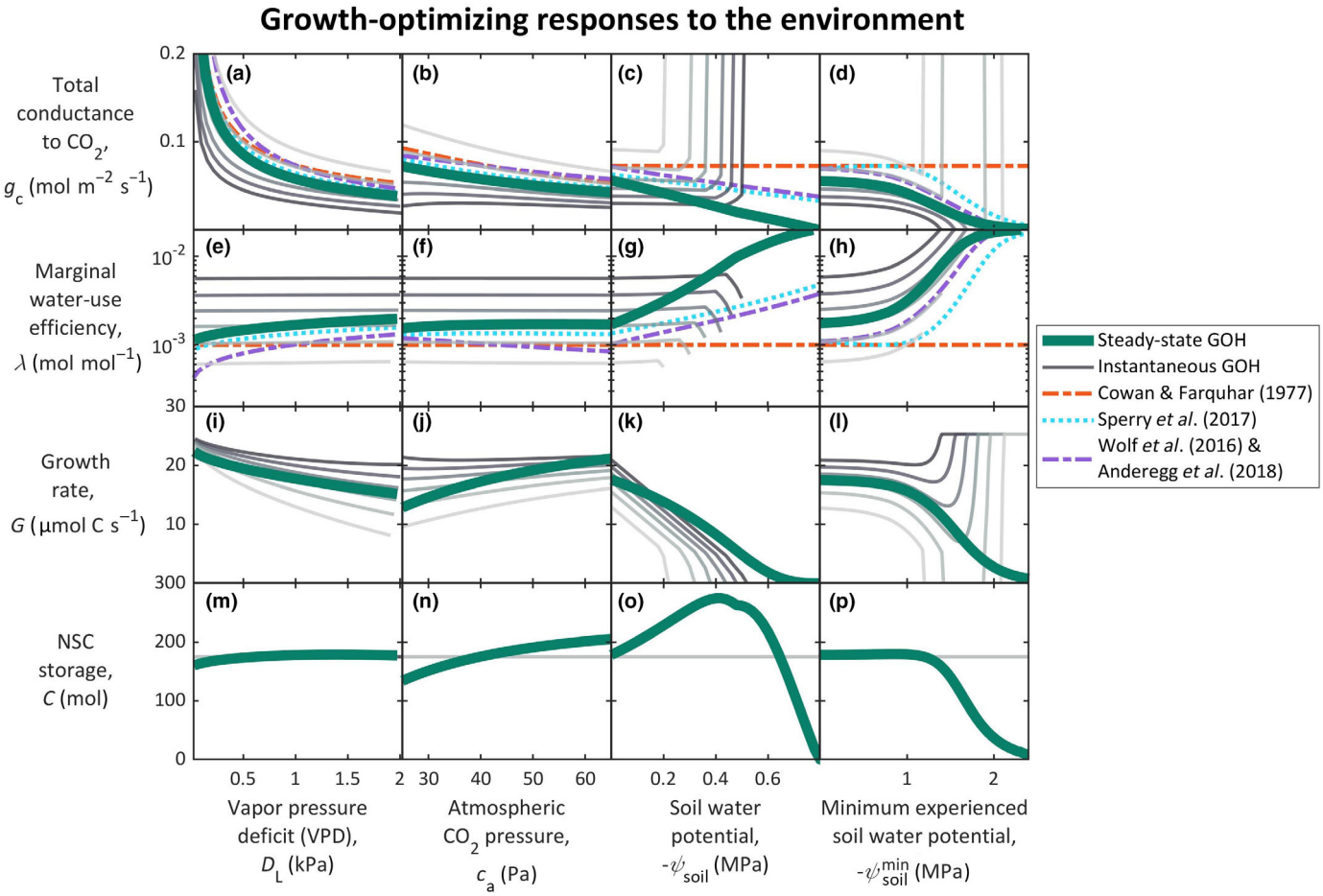


**Fig. 4** Instantaneous and steady-state responses, according to the growth optimization hypothesis (GOH), to varied vapor-pressure deficit (VPD; $D_L$) (a, e, i, m), atmospheric $CO_2$ pressure ($c_a$) (b, f, j, n), soil water potential ($-\psi_{soil}$) (c, g, k, o), and losses in hydraulic conductance (d, h, l, p). Predictions include the optimal total conductance ($g_c$) (a–d), the optimal marginal water-use efficiency ($\lambda$) (e–h), the coinciding growth rate ($G$) (i–l), and the coinciding non-structural carbohydrate (NSC) storage ($C$) (m–p). Instantaneous optimizations were calculated for different NSCUEs ($\eta$) according to the GOH, with $\eta$ ranging from 30% to 80% of its maximum value ($1 - f_c$) in 10% increments (darkest to lightest), and were calculated for an NSC storage based on measurements of Scots pine of similar size as our simulated tree by Schiestl-Aalto *et al*. (2019) ($C = 175$ mol). In (d, h, l, p), conductance was lost as if exposed to a previous drought with magnitude denoted by the minimum experienced soil water potential ($\psi_{soil}^{min}$), assuming that this conductance loss is irrecoverable. Despite the loss of conductance due to past drought (i.e. negative $\psi_{soil}^{min}$), results in (d, h, l, p) represent a tree that is currently well-watered (i.e. $\psi_{soil} = 0$), and thus these results represent postdrought recovery. Sharp increases in the instantaneous $g_c$ under current or past soil water stress in (c, d) (i.e. at more negative $\psi_{soil}$ and $\psi_{soil}^{min}$) result from coinciding instantaneous $\lambda = 0$ in (g, h) and thus also instantaneous $G = 0$ in (k, l). Predictions made by three selected AOHs are shown for comparison.

and AOH predictions are consistent despite differences in their proxies for evolutionary fitness. Mathematical details of the AOHs are presented in the Supporting Information (Notes S1; Section S7), and their parameters are listed in Table 3.

## Results

Both instantaneous and steady-state optimizations predict stomata close as VPD increases (Fig. 4a). Predicted sensitivities of $g_w$ to VPD ($m = -dg_w/d\log_e(D_L)$) from instantaneous and steady-state optimizations agree with reported ranges ($m \approx 0.5$–$0.6$; Oren *et al.*, 1999; Fig. S8). In instantaneous optimizations with large $\eta$, VPD sensitivities are smaller ($m \approx 0.47$) but still realistic (Katul *et al.*, 2009). The instantaneous marginal WUE ($\lambda$) is nearly independent of VPD, except at large $\eta$, when $\lambda$ increases slightly with VPD (Fig. 4e). In steady-state optimizations, increasing VPD resulted in larger $\bar{\lambda}$, slightly more NSCs, and slower growth (Fig. 4e,i,m). Steady-state predictions of $g_c$, $\bar{\lambda}$, and their VPD trends agree well with AOH models (Figs 4a,e, S9a,e), which are all instantaneous in nature. The Prentice *et al.* (2014) model is the only model that predicts $\lambda$ declines slightly with VPD (Fig. S9e).

Both instantaneous and steady-state optimizations predict stomatal closure under $eCO_2$ (Fig. 4b), agreeing with AOH models, except the model by Wolf *et al.* (2016) and Anderegg *et al.* (2018), which is the only model to predict a negative relationship between $\lambda$ and $c_a$ (Figs 4f, S9f; Wang *et al.*, 2020). In instantaneous and steady-state optimizations, $\lambda$ is nearly independent of $c_a$ (Fig. 4f), while some AOH models predict $\lambda$ increases (Figs 4f, S9f). The GOSM can also predict greater increases in $\lambda$

under $eCO_2$ for particular combinations of $\gamma_r$ and $\gamma_g$ (Fig. S10). These combinations of $\gamma_r$ and $\gamma_g$, however, do not necessarily coincide with NSC reserves under ambient and elevated $c_a$ (Figs S6, S7). Regardless of $\gamma_r$ and $\gamma_g$, $eCO_2$ always promotes growth (Fig. S11) and stomatal closure (Fig. S12). Predictions with additional acclimation of $a_L$, $V_{c,max}$, and $J_{max}$ to $eCO_2$ always show an increase in $\lambda$ under $eCO_2$ regardless of $\gamma_r$ and $\gamma_g$ (Fig. S13). Strictly speaking, acclimation of $a_L$, $V_{c,max}$, and $J_{max}$ is an optimal strategy only if it further enhances growth, which is indeed the case (Fig. S14).

Instantaneous solutions for $g_c$ and $\lambda$ are generally independent of $\psi_{soil}$, though they respectively increase and decrease with $\eta$ (Fig. 4c). Beyond a threshold in $\psi_{soil}$, instantaneous $g_c$ dramatically increases and $\lambda$ approaches zero as turgor becomes too small for growth (Fig. 4g,k). Conversely, steady-state optimization predicts $g_c$ and $G$ decrease and $\bar{\lambda}$ increases as soils dry (Fig. 4g). Nonstructural carbohydrates are maximal under moderate soil water stress, because reductions in $A_n$ are smaller than the reduction in $G$, thus elevating NSCs (Fig. 4o). Under extreme stress, NSCs deplete due to strong stomatal limitations to $A_n$ (Fig. 4o). Steady-state predictions of $g_c$ and $\bar{\lambda}$ to soil water stress agree with AOH models (Figs 4c,g, S9c,g), except the Cowan & Farquhar (1977) and Prentice *et al.* (2014) models, both of which require additional parameterizations to describe drought responses (Manzoni *et al.*, 2011; Lavergne *et al.*, 2020a). Steady-state $g_c$ is more sensitive to declines in $\psi_{soil}$ than instantaneous AOH models (Figs 4c, S9c), representing a more conservative water-use strategy in response to soil water stress.

Drought-induced xylem conductance loss induced stomatal closure and increased $\lambda$ during postdrought recovery in both instantaneous and steady-state optimizations (Fig. 4d,h). Near-identical steady-state results are found when conductance hysteresis is modeled by Venturas *et al.*'s (2018) approach, which considers plant hydraulics but not NSCs (Fig. S15). Predictions agree with AOH models regardless of how we modeled conductance hysteresis (Figs 4d,h, S15). The Cowan & Farquhar (1977) and Prentice *et al.* (2014) models, however, consider leaf-level processes only and thus cannot respond to extrafoliar hydraulics (Figs 4d,h, S9d,h). When applying Venturas *et al.*'s (2018) approach to conductance hysteresis, all models behave similarly, even the Cowan & Farquhar (1977) and Prentice *et al.* (2014) models (Fig. S16).

Postdrought growth and whole-tree conductance progressively decline after worsening past droughts (Figs 4l, 5). After moderate droughts ($\psi_{soil}^{min} > c.\ -1.2$ MPa; PLC $< c.$ 78%), NSCs can recover to predrought levels (Figs 4p, 5). After severe droughts ($\psi_{soil}^{min} < c.\ -1.44$ MPa; PLC $> c.$ 85%), NSCs deplete, approaching starvation for $\psi_{soil}^{min} < -2.4$ MPa (Figs 4p, 5). Near-identical postdrought results for growth, conductance, and NSCs are found by Venturas *et al.*'s (2018) approach for conductance hysteresis (Figs S15, S17). These postdrought responses differ remarkably from predictions under permanent water stress (Fig. 5). Under permanent water stress, acclimated NSCs accumulate with PLC between 0% and *c.* 38%, past which NSCs rapidly deplete, approaching NSC depletion when PLC ≈ 47% and soil water stress is only moderate ($\psi_{soil} = -0.8$ MPa; Figs 4o, 5).

## Discussion

### Comparing GOH and AOHs

Here, we hypothesized stomata follow strategies that maximize stem growth over a plant's entire lifetime, which we call the GOH. Integrated over time, maximizing growth further maximizes size, enhancing their ability to compete for resources (King, 1990; Franklin, 2007) and reproduce (Greene & Johnson, 1994;

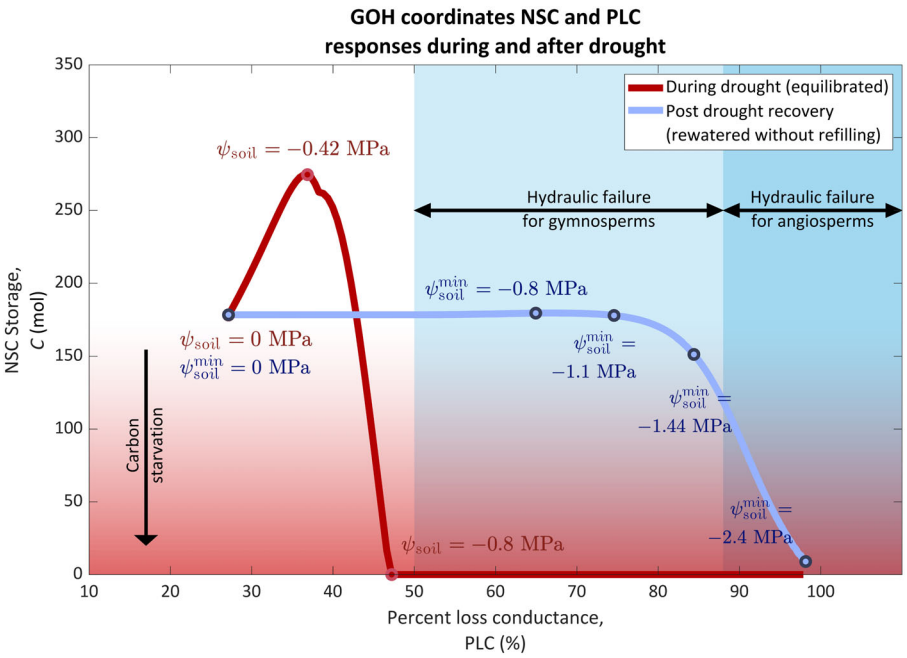


**Fig. 5** Phase diagram of nonstructural carbohydrates (NSCs) and percent loss of whole-plant conductance (PLC) for our simulated Scots pine in equilibrium with varied $\psi_{soil}$ (during drought) and $\psi_{soil}^{min}$ (postdrought recovery; rewatered without refilling of embolisms at $\psi_{soil} = 0$) and other environmental forcing listed in Table 3. Coinciding values of $\psi_{soil}$ and $\psi_{soil}^{min}$ are denoted (circles) to signify the magnitude of soil water stress. Equilibration to $\psi_{soil}$ represents acclimation to permanent soil water stress, while equilibration to $\psi_{soil}^{min}$ represents postdrought recovery, particularly after a transient period of intense soil water stress that leads to irrecoverable embolism. Hydraulic failure is typically associated with a PLC of at least 50% for gymnosperms (Brodribb & Cochard, 2009) and 88% for angiosperms (Resco *et al.*, 2009; Urli *et al.*, 2013).

Obeso, 2002; Minor & Kobe, 2019). We have shown the GOH agrees with our current understanding of stomatal regulation in relation to environmental forcings (Figs 4, S9). We compared these results to the historically prevailing assumption that stomata optimize photosynthetic carbon assimilation in relation to external water availability or internal water stress (e.g. Cowan & Farquhar, 1977; Wolf *et al.*, 2016), which we call AOHs.

All optimization theories assume plants have developed stomatal strategies that maximize evolutionary fitness. This assumption is reasonable, since it springs from natural selection, a core principle of biology (Mäkelä *et al.*, 2002; Franklin *et al.*, 2020). For biologically realistic solutions, AOHs must make a secondary assumption about additional costs or constraints that penalize stomatal opening; otherwise, AOHs would always predict maximal conductance, since $A_n$ is a positive monotonic function of $g_c$ (in the absence of nonstomatal limitations to photosynthesis). These costs and constraints have been associated with water-saving strategies (solved either over short durations; Cowan, 1977; Cowan & Farquhar, 1977; Hari *et al.*, 1986; or dynamically; e.g. Mäkelä *et al.*, 1996; Manzoni *et al.*, 2013), xylem embolism (e.g. Wolf *et al.*, 2016; Sperry *et al.*, 2017), and nonstomatal limitations (e.g. Dewar *et al.*, 2018). Few experiments have attempted to determine the true nature of these costs (Hall & Schulze, 1980; Fites & Teskey, 1988; Thomas *et al.*, 1999; Manzoni *et al.*, 2011). That is, costs are assumed *a priori*, and the validity of those assumptions relies on how well predictions of $g_c$ match observations. The fact that a wide range of assumed costs all converge toward similar responses to environmental cues (Figs 4, S9) demonstrates the difficulty in inferring the true cost from $g_c$ responses. The GOH, on the contrary, does not require assuming additional costs, since the cost of opening stomata is implicit in how plants grow. While opening stomata assimilate carbon as NSCs, which build tissue and generate turgor (Sapes *et al.*, 2021), opening reduces $\psi$ (Sperry *et al.*, 1998) and thus also cambial turgor pressures (Hölttä *et al.*, 2010), thereby hindering the division and expansion of cells (Lockhart, 1965; Kirkham *et al.*, 1972). Hence, the GOH advances turgor-limited growth as a simpler proxy for evolutionary fitness.

Many AOHs maximize their assimilation instantaneously for the immediate environmental conditions without consideration of future resource availability, potentially leading to overly aggressive resource use, hampering future fitness (Lu *et al.*, 2020; Feng *et al.*, 2022). Here, we compared GOH predictions to several instantaneous AOHs (Wolf *et al.*, 2016; Wang *et al.*, 2020), which generally predict biologically correct responses of $g_c$ to environmental stimuli (Wang *et al.*, 2020; Table S2). They compared well to the steady-state predictions of our GOSM, both qualitatively and quantitatively (Figs 4, S9). However, whether instantaneously AOHs truly reflect current conditions or whether they compensate for delayed acclimation to future conditions through their assumed costs ($\lambda$) remains unclear. For example, some AOHs predict an immediate increase in $\lambda$ as soon as exposed to $eCO_2$ (Figs 4f, S9f). However, little is known about how quickly $\lambda$ changes under $eCO_2$ in reality and whether these changes solely reflect stomatal movements. While experiments suggest $\lambda$ indeed increases under $eCO_2$ over multiple years (e.g. Katul *et al.*, 2010), increases in $\lambda$ may reflect other physiological acclimations to $eCO_2$ over longer timescales (Buckley & Schymanski, 2014), including acclimation of photosynthetic capacities, leaf area, and NSC reserves (Ainsworth & Rogers, 2007; Dietze *et al.*, 2014; Lauriks *et al.*, 2021; Fig. S13). Hence, instantaneous AOHs are inappropriate for examining responses to long-term environmental change (Medlyn *et al.*, 2013). If stomata truly maximize growth, then our results would suggest instantaneous AOHs (e.g. Wolf *et al.*, 2016) may predict realistic $g_c$ by approximating foliar acclimations that have not yet occurred.

Our steady-state solution represents the coordination among $g_c$, $G$, and $C$ upon complete acclimation to constant environmental conditions, while the instantaneous solution represents a snapshot in time as $g_c$, $G$, and $C$ transition dynamically from one state to another. The dynamic state represented by the instantaneous solution depends on $\eta$ and $C$ (Figs 3, 4), their temporal evolution (Eqns 2, 9), and the variation in environmental conditions over small timescales. Analogously, our steady-state solution is comparable to observations from long experiments with small variations in the environment and other physiological properties ($a_L$, $V_{c,max}$, $J_{max}$, xylem conductance, allometry, etc.). Our instantaneous solution is comparable to observations from short experiments. However, properly comparing instantaneous solutions to observations would require explicitly modeling the dynamics of $\eta$ and $C$. In steady state, the GOH consistently captured stomatal responses to $D_L$, $c_a$, $\psi_{soil}$, and $\psi_{soil}^{min}$ (Fig. 4a–d), while instantaneous solutions explained only responses to $D_L$ (Fig. 4a), which changes quickly. However, $c_a$, $\psi_{soil}$, and $\psi_{soil}^{min}$ change slowly in reality and likely at rates that are similar to or slower than changes in $\eta$ and/or $C$, which are assumed constant in our instantaneous predictions (Fig. 4). Future work should explore how quickly $\eta$ evolves. Thus, steady state is better than the instantaneous solution for predicting stomatal behavior to slowly changing $c_a$, $\psi_{soil}$, and $\psi_{soil}^{min}$, since steady state approximates the key dynamic feedback between $\eta$, $C$, and the environment.

Interestingly, the GOH predicts the instantaneous marginal WUE ($\chi_w$) is generally near constant over short timescales with respect to potential $g_c$ (Fig. 3a) and over broad environmental conditions (Fig. 4e–g), resulting from growth being a near-linear function of transpiration and $g_c$ ($\partial^2 G_0/\partial E^2 \approx 0$; Fig. 2). Conversely, the GOH predicts the steady-state marginal WUE ($\overline{\chi}_w$) varies strongly with potential $g_c$ (Fig. 3b) with environmental conditions over longer timescales once both $\eta$ and $C$ have equilibrated (Fig. 4e–h). Thus, in the short term, the GOH behaves like the earliest water-saving AOH which specifies a constant $\chi_w$ (Cowan, 1977; Cowan & Farquhar, 1977; Figs 3a, 4), which much evidence supports (Medlyn *et al.*, 2011; Buckley *et al.*, 2017). In the long term, the GOH behaves like recent *Gain-Risk* AOHs, which specify $\chi_w$ (or its related hydraulic cost, $\Theta$; $d\Theta/dE = \chi_w$) depends on environmental conditions and physiological variables (e.g. Wolf *et al.*, 2016; Sperry *et al.*, 2017; Figs 3b–d, 4). The GOH reconciles differences between early and recent AOHs.

Additionally, the GOSM suggests $\chi_w = 0$ when growth cannot occur ($G = 0$) in instantaneous solutions (Fig. 3a), since $\chi_w \propto \partial G_0/\partial E$ (Eqn 8b) and $\partial G_0/\partial E = 0$ when $G_0 = 0$ (Fig. 2).

That is, our instantaneous GOH is maximizing solely $A_n$ without shadow costs ($\Theta = 0$) when plants cannot grow. Nonstomatal limitations should be incorporated into the GOH for these instances and improve predictions when plants cannot grow (Fig. 4g,h) following aspects of AOHs that maximize $A_n$ subject to nonstomatal limitations, since these AOHs implicitly assume $\chi_w = 0$ (Hölttä *et al.*, 2017; Dewar *et al.*, 2018, 2022).

### Xylem embolism and mortality

Stomata have long been theorized to close early under water stress to prevent xylem embolism and conductance loss, thereby inspiring many models which postulate embolism and conductance loss as dominant controls on stomata (e.g. Jones & Sutherland, 1991; Sperry & Love, 2015; Sperry *et al.*, 2016, 2017; Wolf *et al.*, 2016; Eller *et al.*, 2018; Carminati & Javaux, 2020). Under water stress, our GOSM predicts similar results as embolism- and conductance-centric models (Figs 4, S9), though without explicitly minimizing embolism or maximizing conductance. This agreement may not be surprising, considering numerous stomatal strategies inadvertently prevent embolism (Novick *et al.*, 2016; Dewar *et al.*, 2022). While plants indeed tend to operate with minimal embolism and constant xylem conductance (Carminati & Javaux, 2020), this phenomenon does not necessitate that stomata strictly close to prevent embolism and conductance loss. In fact, stomata behave more conservatively than required to prevent significant embolism (Anderegg *et al.*, 2017; Martin-StPaul *et al.*, 2017; Buckley, 2021), suggesting stomata close to maintain other biological functions that are more sensitive to water stress, including turgor maintenance and growth (Hsiao & Acevedo, 1974; Bartlett *et al.*, 2016). Our GOH does not explicitly incorporate embolism prevention or conductance maintenance into its assumptions but nonetheless minimizes embolism and conductance loss. If xylem lost conductance, downstream tissues would have to operate under greater tension, thereby reducing turgor and growth. Hence, stomata close to maximize growth, avoiding conductance losses which would penalize growth.

The prevalence of the idea that stomata operate to prevent embolism and maintain xylem conductance likely originates from widely held notions of how plants die. McDowell *et al.* (2008, 2011) proposed a popular framework in which embolism ultimately leads to desiccation (the so-called *hydraulic failure*) and mortality. Thus, stomata are expected to prevent mortality by moderating embolism and conductance loss. The notion of *hydraulic failure* has stimulated a large number of studies on the degree of embolism past which plants die (e.g. Brodribb & Cochard, 2009; Barigah *et al.*, 2013; Urli *et al.*, 2013; Adams *et al.*, 2017) and how the corresponding $\psi$ threshold varies among species and environments (e.g. Choat *et al.*, 2012; Oliveira *et al.*, 2019; Rosas *et al.*, 2019). However, several recent experimental studies have demonstrated plants can recover despite surpassing these thresholds (Li *et al.*, 2016; Hammond *et al.*, 2019; Mantova *et al.*, 2021), and modeling studies could not identify thresholds to accurately predict mortality in forest stands (De Kauwe *et al.*, 2020; Venturas *et al.*, 2021). These studies cast doubt on embolism as a useful predictor of mortality as well as on whether stomata strictly attempt to prevent embolism. Desiccation (loss of water content and turgor of the meristem and inner bark) is indeed mechanistically linked to mortality (Sapes *et al.*, 2019; Preisler *et al.*, 2021; Sapes & Sala, 2021; Mantova *et al.*, 2022). However, embolism alone cannot describe the critical sequence of events leading up to desiccation and mortality. How quickly the meristem and inner bark desiccates depends not only on the degree of water stress (expressed by $\psi$ or corresponding conductance), but also on the radial conductance between xylem and inner bark (Sevanto *et al.*, 2011; Baert *et al.*, 2015; Preisler *et al.*, 2021), other extra-xylem resistances (e.g. Scoffoni *et al.*, 2017), tissues' water storage capacities (Meinzer *et al.*, 2009; Salomón *et al.*, 2017; Preisler *et al.*, 2022), phloem transport (Chan *et al.*, 2016; Epron *et al.*, 2021), and NSC storage (O'Brien *et al.*, 2014; Sapes *et al.*, 2021). Hence, strategies for avoiding desiccation and mortality depend on complex water and carbon transport processes throughout the plant rather than simply embolism (McDowell *et al.*, 2022). Through the GOH, we offer a general framework to incorporate all of these processes to predict mortality directly from tissue water content as outlined in the Supporting Information (Notes S1; Section S10.2).

Our GOH shifts focus on the predictor of drought-induced mortality from xylem conductance and embolism to turgor (or water content; Notes S1; Sections S2, S10.1, S10.2). Even though it does not include many of the water and carbon transport processes required to predict the time and stress required to desiccate the meristem and kill a plant, our GOSM does represent NSC storage, a key control of survival (O'Brien *et al.*, 2014; Sapes *et al.*, 2021). Thus, our GOSM can predict how percent loss of conductance (PLC) and NSC storage are related for hypothetical drought scenarios (Fig. 5). Though conceptually interdependent (McDowell *et al.*, 2011, 2022), PLC and NSCs are considered two distinct axes for mortality in practice (e.g. Anderegg *et al.*, 2012; Adams *et al.*, 2017). Notably, the GOH provides a link between PLC and NSCs, though the exact relationship differs between during-drought and postdrought conditions (Fig. 5). Conversely, AOHs do not consider NSCs and thus cannot predict such coordination. Though recent studies suggest PLC is not the best predictor of mortality (De Kauwe *et al.*, 2020; Venturas *et al.*, 2021), we nevertheless demonstrate the GOSM's ability to capture fundamental processes and trends between PLC and NSCs (Fig. 5), since a large body of empirical studies of PLC exists to test model predictions. However, we do not focus on the exact values of this PLC–NSC coordination (Fig. 5), which are species- and climate-specific, since we have parameterized the GOSM for a mature Scots pine at a single site (Table 3).

In all cases, plants increasingly embolize as drought worsens, but NSC trends depend on the severity of past and current water stress (Fig. 5). During persistent drought (i.e. long enough for plants to equilibrate; $dC/dt = 0$; $d\eta/dt = 0$), NSCs accumulate under moderate water stress ($\psi_{soil} > -0.42$ MPa) and deplete under severe water stress ($\psi_{soil} < -0.42$ MPa; Fig. 5), explaining conflicting NSC patterns from drought studies (e.g. Galiano *et al.*, 2011; Galvez *et al.*, 2011; Piper, 2011) and observations of NSCs first elevating before later depleting during progressively worsening droughts (e.g. Adams *et al.*, 2013; Mitchell *et al.*, 2014). Our simulated tree

would certainly be incapable of inhabiting environments where $\psi_{soil}$ never exceeded −0.8 MPa due to the inability to maintain minimum NSCs (the so-called *carbon starvation*; Fig. 5). The exact minimum $\psi_{soil}$ trees that could indefinitely tolerate should correspond to their minimum-tolerable tissue water content or turgor, which integrate both PLC and NSCs (Martínez-Vilalta *et al.*, 2019; Sapes *et al.*, 2019). Our GOSM predicts potential turgor if NSCs were nonlimiting, $P_0$, rather than explicitly modeling the true turgor, $P$ (Notes S1; Sections S6, S10.1), and thus we cannot define the exact minimum $\psi_{soil}$ that could be tolerated indefinitely, though it would certainly be more negative than −0.42 MPa (Fig. 5). Improvements to the GOSM would enable explicit prediction of $P$, water content, and thus mortality (Notes S1; Section S10.2). These predictions under long-term water stress may be interpreted as death by *carbon starvation* without *hydraulic failure*, considering *hydraulic failure* would require far more embolism (PLC > 50% for conifers; Brodribb & Cochard, 2009). However, plants rarely die by *carbon starvation* alone (Adams *et al.*, 2017), suggesting steady-state predictions (i.e. $dC/dt = 0$; $d\eta/dt = 0$) of during-drought responses are not appropriate for interpreting mortality.

We also considered how plants operate postdrought with replenished soil water, having lost significant conductance (Anderegg *et al.*, 2012), since mortality often does not occur during the drought itself but lags by several years (Trugman *et al.*, 2018). Hence, postdrought simulations of plants with significant conductance loss (Fig. 5) represent *legacy effects* remaining after drought (Kannenberg *et al.*, 2020). Again, we cannot predict the exact 'point of no return'. Nevertheless, assuming our simulated tree survived the initial drought, the tree can completely recover its NSC reserves even after severe drought ($\psi_{soil}^{min} > -1.2$ MPa), despite suffering PLCs as large as *c.* 80% (Fig. 5). If mortality eventually occurred in this scenario, the death mechanism would be *hydraulic failure* without *carbon starvation*, consistent with some studies (e.g. Anderegg *et al.*, 2012; Garcia-Forner *et al.*, 2017; Kannenberg & Phillips, 2020). After droughts in which $\psi_{soil}^{min} < -1.44$ MPa, simulated trees were incapable of fully recovering their NSC reserves with whole-tree PLCs in excess of 85% regardless of embolism-hysteresis approaches (Figs 4p, 5). Interestingly, this simulated threshold ($\psi_{soil}^{min} = -1.44$) nearly equals the permanent wilting point (classically, $\psi_{soil} = -1.5$ MPa in soil sciences; da Silva *et al.*, 1994). However, this degree of soil water stress may not always challenge plants, since the actual soil wilting point is soil-, plant-, and climate-specific (Torres *et al.*, 2021). For trees eventually dying in this second scenario, the death mechanisms are *hydraulic failure* and *carbon starvation*. Here, PLC and NSCs are negatively correlated, which evidence supports (Adams *et al.*, 2017; Tomasella *et al.*, 2020), signifying the mechanisms' interdependence. These postdrought predictions may explain why *hydraulic failure* is widely observed at death, while dead plants may or may not suffer *carbon starvation* (Adams *et al.*, 2017).

## Acknowledgements

AP and XF acknowledge the support from the National Science Foundation CAREER award DEB-2045610. We thank Antoine Cabon and Gerard Sapes for commentating on an early version of the manuscript. We are grateful to Tom Buckley and two other anonymous reviewers who provided suggestions and insights to improve the manuscript.

## Competing interests

None declared.

## Author contributions

AP and XF designed the model and simulation experiments. AP coded and ran the model, analyzed simulated data, and led the writing. All authors contributed to data interpretation, discussion, figure preparation, and the final version.

## ORCID

Xue Feng https://orcid.org/0000-0003-1381-3118
Aaron Potkay https://orcid.org/0000-0003-3101-2701

## Data availability

MATLAB codes for model and plotting/analyzing data, including forcing data, and simulation outputs are available in Notes S2.

## References

**Adams HD, Germino MJ, Breshears DD, Barron-Gafford GA, Guardiola-Claramonte M, Zou CB, Huxman TE. 2013.** Nonstructural leaf carbohydrate dynamics of *Pinus edulis* during drought-induced tree mortality reveal role for carbon metabolism in mortality mechanism. *New Phytologist* **197**: 1142–1151.

**Adams HD, Zeppel MJ, Anderegg WR, Hartmann H, Landhäusser SM, Tissue DT, Huxman TE, Hudson PJ, Franz TE, Allen CD *et al.* 2017.** A multi-species synthesis of physiological mechanisms in drought-induced tree mortality. *Nature Ecology & Evolution* **1**: 1285–1291.

**Ainsworth EA, Rogers A. 2007.** The response of photosynthesis and stomatal conductance to rising [$CO_2$]: mechanisms and environmental interactions. *Plant, Cell & Environment* **30**: 258–270.

**Anderegg WR, Berry JA, Smith DD, Sperry JS, Anderegg LD, Field CB. 2012.** The roles of hydraulic and carbon stress in a widespread climate-induced forest die-off. *Proceedings of the National Academy of Sciences, USA* **109**: 233–237.

**Anderegg WR, Wolf A, Arango-Velez A, Choat B, Chmura DJ, Jansen S, Kolb T, Li S, Meinzer F, Pita P *et al.* 2017.** Plant water potential improves prediction of empirical stomatal models. *PLoS ONE* **12**: e0185481.

**Anderegg WR, Wolf A, Arango-Velez A, Choat B, Chmura DJ, Jansen S, Kolb T, Li S, Meinzer FC, Pita P *et al.* 2018.** Woody plants optimise stomatal behaviour relative to hydraulic risk. *Ecology Letters* **21**: 968–977.

**Baert A, De Schepper V, Steppe K. 2015.** Variable hydraulic resistances and their impact on plant drought response modelling. *Tree Physiology* **35**: 439–449.

**Ball JT, Woodrow IE, Berry JA. 1987.** A model predicting stomatal conductance and its contribution to the control of photosynthesis under different environmental conditions. In: Biggins J, ed. *Progress in photosynthesis research*. Dordrecht, the Netherlands: Springer, 221–224.

**Barigah TS, Charrier O, Douris M, Bonhomme M, Herbette S, Améglio T, Fichot R, Brignolas F, Cochard H. 2013.** Water stress-induced xylem hydraulic failure is a causal factor of tree mortality in beech and poplar. *Annals of Botany* **112**: 1431–1437.

**Bartlett MK, Detto M, Pacala SW. 2019.** Predicting shifts in the functional composition of tropical forests under increased drought and $CO_2$ from trade-offs among plant hydraulic traits. *Ecology Letters* **22**: 67–77.

**Bartlett MK, Klein T, Jansen S, Choat B, Sack L. 2016.** The correlations and sequence of plant stomatal, hydraulic, and wilting responses to drought. *Proceedings of the National Academy of Sciences, USA* **113**: 13098–13103.

**Betts RA, Boucher O, Collins M, Cox PM, Falloon PD, Gedney N, Hemming DL, Huntingford C, Jones CD, Sexton DMH *et al.* 2007.** Projected increase in continental runoff due to plant responses to increasing carbon dioxide. *Nature* **448**: 1037–1041.

**Betts RA, Cox PM, Woodward FI. 2000.** Simulated responses of potential vegetation to doubled-$CO_2$ climate change and feedbacks on near-surface temperature. *Global Ecology and Biogeography* **9**: 171–180.

**Brodribb TJ, Cochard H. 2009.** Hydraulic failure defines the recovery and point of death in water-stressed conifers. *Plant Physiology* **149**: 575–584.

**Buckley TN. 2021.** *The role of hydraulic constraints in optimal stomatal behavior* [Conference presentation]. European Geosciences Union [Webinar]. [WWW document] URL https://video.ucdavis.edu/media/EGU+talk+%28TN+Buckley+April+2021%29/1_9atv3crc/25823442 [accessed 1 September 2021].

**Buckley TN, Miller JM, Farquhar GD. 2002.** The mathematics of linked optimisation for water and nitrogen use in a canopy. *Silva Fennica* **36**: 639–669.

**Buckley TN, Mott KA, Farquhar GD. 2003.** A hydromechanical and biochemical model of stomatal conductance. *Plant, Cell & Environment* **26**: 1767–1785.

**Buckley TN, Roberts DW. 2006a.** DESPOT, a process-based tree growth model that allocates carbon to maximize carbon gain. *Tree Physiology* **26**: 129–144.

**Buckley TN, Roberts DW. 2006b.** How should leaf area, sapwood area and stomatal conductance vary with tree height to maximize growth? *Tree Physiology* **26**: 145–157.

**Buckley TN, Sack L, Farquhar GD. 2017.** Optimal plant water economy. *Plant, Cell & Environment* **40**: 881–896.

**Buckley TN, Schymanski SJ. 2014.** Stomatal optimisation in relation to atmospheric $CO_2$. *New Phytologist* **201**: 372–377.

**Buckley TN, Turnbull TL, Adams MA. 2012.** Simple models for stomatal conductance derived from a process model: cross-validation against sap flux data. *Plant, Cell & Environment* **35**: 1647–1662.

**Cabon A, Kannenberg SA, Arain A, Babst F, Baldocchi D, Belmecheri S, Delpierre N, Guerrieri R, Maxwell JT, McKenzie S *et al.* 2022.** Cross-biome synthesis of source versus sink limits to tree growth. *Science* **376**: 758–761.

**Cabon A, Peters RL, Fonti P, Martínez-Vilalta J, De Cáceres M. 2020.** Temperature and water potential co-limit stem cambial activity along a steep elevational gradient. *New Phytologist* **226**: 1325–1340.

**Cailleret M, Jansen S, Robert EM, Desoto L, Aakala T, Antos JA, Beikircher B, Bigler C, Bugmann H, Caccianiga M *et al.* 2017.** A synthesis of radial growth patterns preceding tree mortality. *Global Change Biology* **23**: 1675–1690.

**Carminati A, Javaux M. 2020.** Soil rather than xylem vulnerability controls stomatal response to drought. *Trends in Plant Science* **25**: 868–880.

**Chan T, Hölttä T, Berninger F, Mäkinen H, Nöjd P, Mencuccini M, Nikinmaa E. 2016.** Separating water-potential induced swelling and shrinking from measured radial stem variations reveals a cambial growth and osmotic concentration signal. *Plant, Cell & Environment* **39**: 233–244.

**Choat B, Jansen S, Brodribb TJ, Cochard H, Delzon S, Bhaskar R, Bucci SJ, Feild TS, Gleason SM, Hacke UG *et al.* 2012.** Global convergence in the vulnerability of forests to drought. *Nature* **491**: 752–755.

**Chung HH, Barnes RL. 1977.** Photosynthate allocation in *Pinus taeda taeda*. I. Substrate requirements for synthesis of shoot biomass. *Canadian Journal of Forest Research* **7**: 106–111.

**Collalti A, Ibrom A, Stockmarr A, Cescatti A, Alkama R, Fernández-Martínez M, Matteucci G, Sitch S, Friedlingstein P, Ciais P *et al.* 2020.** Forest production efficiency increases with growth temperature. *Nature Communications* **11**: 1–9.

**Collatz GJ, Ball JT, Grivet C, Berry JA. 1991.** Physiological and environmental regulation of stomatal conductance, photosynthesis and transpiration: a model that includes a laminar boundary layer. *Agricultural and Forest Meteorology* **54**: 107–136.

**Collins AD, Ryan MG, Adams HD, Dickman LT, Garcia-Forner N, Grossiord C, Powers HH, Sevanto S, McDowell NG. 2021.** Foliar respiration is related to photosynthetic, growth and carbohydrate response to experimental drought and elevated temperature. *Plant, Cell & Environment* **44**: 3623–3635.

**Cowan IR. 1977.** Stomatal behaviour and environment. *Advances in Botanical Research* **4**: 117–228.

**Cowan IR. 1982.** Regulation of water use in relation to carbon gain in higher plants. In: Lange OL, Nobel PS, Osmond CB, Ziegler H, eds. *Physiological plant ecology II*. Berlin & Heidelberg, Germany: Springer, 589–613.

**Cowan IR, Farquhar GD. 1977.** Stomatal function in relation to leaf metabolism and environment. In: Jennings DH, ed. *Integration of activity in the higher plant*. Cambridge, UK: Cambridge University Press, 471–505.

**Cox PM, Betts RA, Jones CD, Spall SA, Totterdell IJ. 2000.** Acceleration of global warming due to carbon-cycle feedbacks in a coupled climate model. *Nature* **408**: 184–187.

**Das AJ, Stephenson NL, Davis KP. 2016.** Why do trees die? Characterizing the drivers of background tree mortality. *Ecology* **97**: 2616–2627.

**De Kauwe MG, Kala J, Lin YS, Pitman AJ, Medlyn BE, Duursma RA, Abramowitz G, Wang Y, Miralles DG. 2015.** A test of an optimal stomatal conductance scheme within the CABLE land surface model. *Geoscientific Model Development* **8**: 431–452.

**De Kauwe MG, Medlyn BE, Ukkola AM, Mu M, Sabot ME, Pitman AJ, Meir P, Cernusak LA, Rifai SW, Choat B *et al.* 2020.** Identifying areas at risk of drought-induced tree mortality across South-Eastern Australia. *Global Change Biology* **26**: 5716–5733.

**De Pury DGG, Farquhar GD. 1997.** Simple scaling of photosynthesis from leaves to canopies without the errors of big-leaf models. *Plant, Cell & Environment* **20**: 537–557.

**De Schepper V, Steppe K. 2010.** Development and verification of a water and sugar transport model using measured stem diameter variations. *Journal of Experimental Botany* **61**: 2083–2099.

**Deans RM, Brodribb TJ, Busch FA, Farquhar GD. 2020.** Optimization can provide the fundamental link between leaf photosynthesis, gas exchange and water relations. *Nature Plants* **6**: 1116–1125.

**DeSoto L, Cailleret M, Sterck F, Jansen S, Kramer K, Robert EM, Aakala T, Amoroso MM, Bigler C, Camarero JJ *et al.* 2020.** Low growth resilience to drought is related to future mortality risk in trees. *Nature Communications* **11**: 545.

**Dewar R, Hölttä T, Salmon Y. 2022.** Exploring optimal stomatal control under alternative hypotheses for the regulation of plant sources and sinks. *New Phytologist* **233**: 639–654.

**Dewar R, Mauranen A, Mäkelä A, Hölttä T, Medlyn B, Vesala T. 2018.** New insights into the covariation of stomatal, mesophyll and hydraulic conductances from optimization models incorporating nonstomatal limitations to photosynthesis. *New Phytologist* **217**: 571–585.

**Dietze MC, Sala A, Carbone MS, Czimczik CI, Mantooth JA, Richardson AD, Vargas R. 2014.** Nonstructural carbon in woody plants. *Annual Review of Plant Biology* **65**: 667–687.

**Domec JC, Palmroth S, Ward E, Maier CA, Therezien M, Oren R. 2009.** Acclimation of leaf hydraulic conductance and stomatal conductance of *Pinus taeda* (loblolly pine) to long-term growth in elevated $CO_2$ (free-air $CO_2$ enrichment) and N-fertilization. *Plant, Cell & Environment* **32**: 1500–1512.

**Eller CB, Rowland L, Mencuccini M, Rosas T, Williams K, Harper A, Medlyn BE, Wagner Y, Klein T, Teodoro GS *et al.* 2020.** Stomatal optimization based on xylem hydraulics (SOX) improves land surface model simulation of vegetation responses to climate. *New Phytologist* **226**: 1622–1637.

**Eller CB, Rowland L, Oliveira RS, Bittencourt PR, Barros FV, Da Costa AC, Meir P, Friend AD, Mencuccini M, Sitch S *et al.* 2018.** Modelling tropical forest responses to drought and El Niño with a stomatal optimization model based on xylem hydraulics. *Philosophical Transactions of the Royal Society of London. Series B: Biological Sciences* **373**: 20170315.

**Epron D, Bahn M, Derrien D, Lattanzi FA, Pumpanen J, Gessler A, Högberg P, Maillard P, Dannoura M, Gérant D *et al.* 2012.** Pulse-labelling trees to study carbon allocation dynamics: a review of methods, current knowledge and future prospects. *Tree Physiology* **32**: 776–798.

**Epron D, Kamakura M, Azuma W, Dannoura M, Kosugi Y. 2021.** Diurnal variations in the thickness of the inner bark of tree trunks in relation to xylem water potential and phloem turgor. *Plant–Environment Interactions* **2**: 112–124.

**Evans JR, Farquhar GD. 1991.** Modelling canopy photosynthesis from the biochemistry of the C, chloroplast. In: Boote KJ, Loomis RS, eds. *Modelling*

*crop photosynthesis – from biochemistry to canopy, special publication no. 19.* Madison, WI, USA: CSS A, 1–16.

**Fan Y, Miguez-Macho G, Jobbágy EG, Jackson RB, Otero-Casal C. 2017.** Hydrologic regulation of plant rooting depth. *Proceedings of the National Academy of Sciences, USA* **114**: 10572–10577.

**Farquhar GD, von Caemmerer SV, Berry JA. 1980.** A biochemical model of photosynthetic $CO_2$ assimilation in leaves of $C_3$ species. *Planta* **149**: 78–90.

**Farquhar GD, Wong SC. 1984.** An empirical model of stomatal conductance. *Functional Plant Biology* **11**: 191–210.

**Feng X, Lu Y, Jiang M, Katul G, Manzoni S, Mrad A, Vico G. 2022.** Instantaneous stomatal optimization results in suboptimal carbon gain due to legacy effects. *Plant, Cell & Environment* **45**: 3189–3204.

**Feng X, Porporato A, Rodriguez-Iturbe I. 2015.** Stochastic soil water balance under seasonal climates. *Proceedings of the Royal Society A: Mathematical, Physical and Engineering Sciences* **471**: 20140623.

**Fites JA, Teskey RO. 1988.** $CO_2$ and water vapor exchange of *Pinus taeda* in relation to stomatal behavior: test of an optimization hypothesis. *Canadian Journal of Forest Research* **18**: 150–157.

**Forrester DI. 2021.** Does individual-tree biomass growth increase continuously with tree size? *Forest Ecology and Management* **481**: 118717.

**Franklin O. 2007.** Optimal nitrogen allocation controls tree responses to elevated $CO_2$. *New Phytologist* **174**: 811–822.

**Franklin O, Harrison SP, Dewar R, Farrior CE, Brännström Å, Dieckmann U, Pietsch S, Falster D, Cramer W, Loreau M *et al.* 2020.** Organizing principles for vegetation dynamics. *Nature Plants* **6**: 444–453.

**Galiano L, Martínez-Vilalta J, Lloret F. 2011.** Carbon reserves and canopy defoliation determine the recovery of Scots pine 4 yr after a drought episode. *New Phytologist* **190**: 750–759.

**Galvez DA, Landhäusser SM, Tyree MT. 2011.** Root carbon reserve dynamics in aspen seedlings: does simulated drought induce reserve limitation? *Tree Physiology* **31**: 250–257.

**Garcia-Forner N, Biel C, Savé R, Martínez-Vilalta J. 2017.** Isohydric species are not necessarily more carbon limited than anisohydric species during drought. *Tree Physiology* **37**: 441–455.

**Givnish TJ. 1986.** Optimal stomatal conductance, allocation of energy between leaves and roots, and the marginal cost of transpiration. In: Givnish TJ, ed. *On the economy of plant form and function: proceedings of the Sixth Maria Moors Cabot symposium, evolutionary constraints on primary productivity, adaptive patterns of energy capture in plants, Harvard Forest, August 1983.* Cambridge, UK: Cambridge University Press, 171–213.

**Givnish TJ, Vermeij GJ. 1976.** Sizes and shapes of liane leaves. *The American Naturalist* **110**: 743–778.

**Greene DF, Johnson EA. 1994.** Estimating the mean annual seed production of trees. *Ecology* **75**: 642–647.

**Hall AE, Schulze ED. 1980.** Stomatal response to environment and a possible interrelation between stomatal effects on transpiration and $CO_2$ assimilation. *Plant, Cell & Environment* **3**: 467–474.

**Hammond WM, Yu K, Wilson LA, Will RE, Anderegg WR, Adams HD. 2019.** Dead or dying? Quantifying the point of no return from hydraulic failure in drought-induced tree mortality. *New Phytologist* **223**: 1834–1843.

**Hari P, Kulmala M. 2005.** Station for measuring ecosystem–atmosphere relations (SMEAR II). *Boreal Environment Research* **10**: 315–322.

**Hari P, Mäkelä A, Korpilahti E, Holmberg M. 1986.** Optimal control of gas exchange. *Tree Physiology* **2**: 169–175.

**Harley PC, Baldocchi DD. 1995.** Scaling carbon dioxide and water vapour exchange from leaf to canopy in a deciduous forest. I. Leaf model parametrization. *Plant, Cell & Environment* **18**: 1146–1156.

**Hayat A, Hacket-Pain AJ, Pretzsch H, Rademacher TT, Friend AD. 2017.** Modeling tree growth taking into account carbon source and sink limitations. *Frontiers in Plant Science* **8**: 182.

**Hetherington AM, Woodward FI. 2003.** The role of stomata in sensing and driving environmental change. *Nature* **424**: 901–908.

**Hoch G, Richter A, Körner C. 2003.** Non-structural carbon compounds in temperate forest trees. *Plant, Cell & Environment* **26**: 1067–1081.

**Hölttä T, Kurppa M, Nikinmaa E. 2013.** Scaling of xylem and phloem transport capacity and resource usage with tree size. *Frontiers in Plant Science* **4**: 496.

**Hölttä T, Lintunen A, Chan T, Mäkelä A, Nikinmaa E. 2017.** A steady-state stomatal model of balanced leaf gas exchange, hydraulics and maximal source–sink flux. *Tree Physiology* **37**: 851–868.

**Hölttä T, Mäkinen H, Nöjd P, Mäkelä A, Nikinmaa E. 2010.** A physiological model of softwood cambial growth. *Tree Physiology* **30**: 1235–1252.

**Hsiao TC, Acevedo E. 1974.** Plant responses to water deficits, water-use efficiency, and drought resistance. *Developments in Agricultural and Managed Forest Ecology* **1**: 59–84.

**Janssens IA, Sampson DA, Cermak J, Meiresonne L, Riguzzi F, Overloop S, Ceulemans R. 1999.** Above- and belowground phytomass and carbon storage in a Belgian Scots pine stand. *Annals of Forest Science* **56**: 81–90.

**Johnson FH, Eyring H, Williams RW. 1942.** The nature of enzyme inhibitions in bacterial luminescence: sulfanilamide, urethane, temperature and pressure. *Journal of Cellular and Comparative Physiology* **20**: 247–268.

**Jones HG, Sutherland RA. 1991.** Stomatal control of xylem embolism. *Plant, Cell & Environment* **14**: 607–612.

**Jones S, Rowland L, Cox P, Hemming D, Wiltshire A, Williams K, Parazoo N, Liu J, Costa AC, Meir P *et al.* 2020.** The impact of a simple representation of non-structural carbohydrates on the simulated response of tropical forests to drought. *Biogeosciences* **17**: 3589–3612.

**Kannenberg SA, Phillips RP. 2020.** Non-structural carbohydrate pools not linked to hydraulic strategies or carbon supply in tree saplings during severe drought and subsequent recovery. *Tree Physiology* **40**: 259–271.

**Kannenberg SA, Schwalm CR, Anderegg WR. 2020.** Ghosts of the past: how drought legacy effects shape forest functioning and carbon cycling. *Ecology Letters* **23**: 891–901.

**Katul G, Manzoni S, Palmroth S, Oren R. 2010.** A stomatal optimization theory to describe the effects of atmospheric $CO_2$ on leaf photosynthesis and transpiration. *Annals of Botany* **105**: 431–442.

**Katul GG, Palmroth S, Oren RAM. 2009.** Leaf stomatal responses to vapour pressure deficit under current and $CO_2$-enriched atmosphere explained by the economics of gas exchange. *Plant, Cell & Environment* **32**: 968–979.

**King DA. 1990.** The adaptive significance of tree height. *The American Naturalist* **135**: 809–828.

**Kirkham MB, Gardner WR, Gerloff GC. 1972.** Regulation of cell division and cell enlargement by turgor pressure. *Plant Physiology* **49**: 961–962.

**Kolari P, Chan T, Porcar-Castell A, Bäck J, Nikinmaa E, Juurola E. 2014.** Field and controlled environment measurements show strong seasonal acclimation in photosynthesis and respiration potential in boreal Scots pine. *Frontiers in Plant Science* **5**: 717.

**Körner C. 2008.** Winter crop growth at low temperature may hold the answer for alpine treeline formation. *Plant Ecology and Diversity* **1**: 3–11.

**Lauriks F, Salomón RL, Steppe K. 2021.** Temporal variability in tree responses to elevated atmospheric $CO_2$. *Plant, Cell & Environment* **44**: 1292–1310.

**Lavergne A, Sandoval D, Hare VJ, Graven H, Prentice IC. 2020a.** Impacts of soil water stress on the acclimated stomatal limitation of photosynthesis: insights from stable carbon isotope data. *Global Change Biology* **26**: 7158–7172.

**Lavergne A, Voelker S, Csank A, Graven H, de Boer HJ, Daux V, Robertson I, Dorado-Liñán I, Martínez-Sancho E, Battipaglia G *et al.* 2020b.** Historical changes in the stomatal limitation of photosynthesis: empirical support for an optimality principle. *New Phytologist* **225**: 2484–2497.

**Leipprand A, Gerten D. 2006.** Global effects of doubled atmospheric $CO_2$ content on evapotranspiration, soil moisture and runoff under potential natural vegetation. *Hydrological Sciences Journal* **51**: 171–185.

**Leuning R. 1995.** A critical appraisal of a combined stomatal-photosynthesis model for $C_3$ plants. *Plant, Cell & Environment* **18**: 339–355.

**Li S, Feifel M, Karimi Z, Schuldt B, Choat B, Jansen S. 2016.** Leaf gas exchange performance and the lethal water potential of five European species during drought. *Tree Physiology* **36**: 179–192.

**Li W, Hartmann H, Adams HD, Zhang H, Jin C, Zhao C, Guan D, Wang A, Yuan F, Wu J. 2018.** The sweet side of global change–dynamic responses of non-structural carbohydrates to drought, elevated $CO_2$ and nitrogen fertilization in tree species. *Tree Physiology* **38**: 1706–1723.

**Lintunen A, Paljakka T, Salmon Y, Dewar R, Riikonen A, Hölttä T. 2020.** The influence of soil temperature and water content on belowground hydraulic

conductance and leaf gas exchange in mature trees of three boreal species. *Plant, Cell & Environment* **43**: 532–547.

**Lockhart JA. 1965.** An analysis of irreversible plant cell elongation. *Journal of Theoretical Biology* **8**: 264–275.

**Lu Y, Duursma RA, Farrior CE, Medlyn BE, Feng X. 2020.** Optimal stomatal drought response shaped by competition for water and hydraulic risk can explain plant trait covariation. *New Phytologist* **225**: 1206–1217.

**Lu Y, Duursma RA, Medlyn BE. 2016.** Optimal stomatal behaviour under stochastic rainfall. *Journal of Theoretical Biology* **394**: 160–171.

**Mackay DS, Roberts DE, Ewers BE, Sperry JS, McDowell NG, Pockman WT. 2015.** Interdependence of chronic hydraulic dysfunction and canopy processes can improve integrated models of tree response to drought. *Water Resources Research* **51**: 6156–6176.

**Mäkelä A. 1985.** Differential games in evolutionary theory: height growth strategies of trees. *Theoretical Population Biology* **27**: 239–267.

**Mäkelä A, Berninger F, Hari P. 1996.** Optimal control of gas exchange during drought: theoretical analysis. *Annals of Botany* **77**: 461–468.

**Mäkelä A, Givnish TJ, Berninger F, Buckley TN, Farquhar GD, Hari P. 2002.** Challenges and opportunities of the optimality approach in plant ecology. *Silva Fennica* **36**: 605–614.

**Mantova M, Herbette S, Cochard H, Torres-Ruiz JM. 2022.** Hydraulic failure and tree mortality: from correlation to causation. *Trends in Plant Science* **27**: 335–345.

**Mantova M, Menezes-Silva PE, Badel E, Cochard H, Torres-Ruiz JM. 2021.** The interplay of hydraulic failure and cell vitality explains tree capacity to recover from drought. *Physiologia Plantarum* **172**: 247–257.

**Manzoni S, Vico G, Katul G, Fay PA, Polley W, Palmroth S, Porporato A. 2011.** Optimizing stomatal conductance for maximum carbon gain under water stress: a meta-analysis across plant functional types and climates. *Functional Ecology* **25**: 456–467.

**Manzoni S, Vico G, Palmroth S, Porporato A, Katul G. 2013.** Optimization of stomatal conductance for maximum carbon gain under dynamic soil moisture. *Advances in Water Resources* **62**: 90–105.

**Marshall JD, Waring RH. 1985.** Predicting fine root production and turnover by monitoring root starch and soil temperature. *Canadian Journal of Forest Research* **15**: 791–800.

**Martínez-Vilalta J, Anderegg WR, Sapes G, Sala A. 2019.** Greater focus on water pools may improve our ability to understand and anticipate drought-induced mortality in plants. *New Phytologist* **223**: 22–32.

**Martínez-Vilalta J, Cochard H, Mencuccini M, Sterck F, Herrero A, Korhonen JFJ, Llorens P, Nikinmaa E, Nolè A, Poyatos R *et al.* 2009.** Hydraulic adjustment of Scots pine across Europe. *New Phytologist* **184**: 353–364.

**Martínez-Vilalta J, Korakaki E, Vanderklein D, Mencuccini M. 2007.** Below-ground hydraulic conductance is a function of environmental conditions and tree size in Scots pine. *Functional Ecology* **21**: 1072–1083.

**Martínez-Vilalta J, Sala A, Asensio D, Galiano L, Hoch G, Palacio S, Piper FI, Lloret F. 2016.** Dynamics of non-structural carbohydrates in terrestrial plants: a global synthesis. *Ecological Monographs* **86**: 495–516.

**Martin-StPaul N, Delzon S, Cochard H. 2017.** Plant resistance to drought depends on timely stomatal closure. *Ecology Letters* **20**: 1437–1447.

**McDowell N, Pockman WT, Allen CD, Breshears DD, Cobb N, Kolb T, Plaut J, Sperry J, West A, Williams DG *et al.* 2008.** Mechanisms of plant survival and mortality during drought: why do some plants survive while others succumb to drought? *New Phytologist* **178**: 719–739.

**McDowell NG, Beerling DJ, Breshears DD, Fisher RA, Raffa KF, Stitt M. 2011.** The interdependence of mechanisms underlying climate-driven vegetation mortality. *Trends in Ecology & Evolution* **26**: 523–532.

**McDowell NG, Sapes G, Pivovaroff A, Adams HD, Allen CD, Anderegg WR, Arend M, Breshears DD, Brodribb T, Choat B *et al.* 2022.** Mechanisms of woody-plant mortality under rising drought, $CO_2$ and vapour pressure deficit. *Nature Reviews Earth & Environment* **3**: 294–308.

**Medlyn BE, Duursma RA, De Kauwe MG, Prentice IC. 2013.** The optimal stomatal response to atmospheric $CO_2$ concentration: alternative solutions, alternative interpretations. *Agricultural and Forest Meteorology* **182**: 200–203.

**Medlyn BE, Duursma RA, Eamus D, Ellsworth DS, Prentice IC, Barton CV, Crous KY, De Angelis P, Freeman M, Wingate L. 2011.** Reconciling the optimal and empirical approaches to modelling stomatal conductance. *Global Change Biology* **17**: 2134–2144.

**Meinzer FC, Johnson DM, Lachenbruch B, McCulloh KA, Woodruff DR. 2009.** Xylem hydraulic safety margins in woody plants: coordination of stomatal control of xylem tension with hydraulic capacitance. *Functional Ecology* **23**: 922–930.

**Mencuccini M, Grace J. 1996.** Hydraulic conductance, light interception and needle nutrient concentration in Scots pine stands and their relations with net primary productivity. *Tree Physiology* **16**: 459–468.

**Michel BE. 1972.** Solute potentials of sucrose solutions. *Plant Physiology* **50**: 196.

**Minor DM, Kobe RK. 2019.** Fruit production is influenced by tree size and size-asymmetric crowding in a wet tropical forest. *Ecology and Evolution* **9**: 1458–1472.

**Mitchell PJ, O'Grady AP, Tissue DT, Worledge D, Pinkard EA. 2014.** Co-ordination of growth, gas exchange and hydraulics define the carbon safety margin in tree species with contrasting drought strategies. *Tree Physiology* **34**: 443–458.

**Mrad A, Sevanto S, Domec JC, Liu Y, Nakad M, Katul G. 2019.** A dynamic optimality principle for water use strategies explains isohydric to anisohydric plant responses to drought. *Frontiers in Forests and Global Change* **2**: 49.

**Münch E. 1930.** *Die stoffbewegungen in der pflanze.* Jena, Germany: Gustav Fischer.

**Murty D, McMurtrie RE, Ryan MG. 1996.** Declining forest productivity in aging forest stands: a modeling analysis of alternative hypotheses. *Tree Physiology* **16**: 187–200.

**Nikinmaa E, Hölttä T, Hari P, Kolari P, Mäkelä A, Sevanto S, Vesala T. 2013.** Assimilate transport in phloem sets conditions for leaf gas exchange. *Plant, Cell & Environment* **36**: 655–669.

**Novick KA, Miniat CF, Vose JM. 2016.** Drought limitations to leaf-level gas exchange: results from a model linking stomatal optimization and cohesion–tension theory. *Plant, Cell & Environment* **39**: 583–596.

**O'Brien MJ, Leuzinger S, Philipson CD, Tay J, Hector A. 2014.** Drought survival of tropical tree seedlings enhanced by non-structural carbohydrate levels. *Nature Climate Change* **4**: 710–714.

**Obeso JR. 2002.** The costs of reproduction in plants. *New Phytologist* **155**: 321–348.

**Oliveira RS, Costa FR, van Baalen E, de Jonge A, Bittencourt PR, Almanza Y, Barros FV, Cordoba EC, Fagundes MV, Garcia S *et al.* 2019.** Embolism resistance drives the distribution of Amazonian rainforest tree species along hydro-topographic gradients. *New Phytologist* **221**: 1457–1465.

**Oren R, Sperry JS, Katul GG, Pataki DE, Ewers BE, Phillips N, Schäfer KVR. 1999.** Survey and synthesis of intra- and interspecific variation in stomatal sensitivity to vapour pressure deficit. *Plant, Cell & Environment* **22**: 1515–1526.

**Paljakka T, Jyske T, Lintunen A, Aaltonen H, Nikinmaa E, Hölttä T. 2017.** Gradients and dynamics of inner bark and needle osmotic potentials in Scots pine (*Pinus sylvestris* L.) and Norway spruce (*Picea abies* L. Karst). *Plant, Cell & Environment* **40**: 2160–2173.

**Parent B, Turc O, Gibon Y, Stitt M, Tardieu F. 2010.** Modelling temperature compensated physiological rates, based on the co-ordination of responses to temperature of developmental processes. *Journal of Experimental Botany* **61**: 2057–2069.

**Peters RL, Steppe K, Cuny HE, De Pauw DJ, Frank DC, Schaub M, Rathgeber CBK, Cabon A, Fonti P. 2021.** Turgor – a limiting factor for radial growth in mature conifers along an elevational gradient. *New Phytologist* **229**: 213–229.

**Piper FI. 2011.** Drought induces opposite changes in the concentration of non-structural carbohydrates of two evergreen *Nothofagus* species of differential drought resistance. *Annals of Forest Science* **68**: 415–424.

**Poorter H, Niklas KJ, Reich PB, Oleksyn J, Poot P, Mommer L. 2012.** Biomass allocation to leaves, stems and roots: meta-analyses of interspecific variation and environmental control. *New Phytologist* **193**: 30–50.

**Potkay A, Hölttä T, Trugman AT, Fan Y. 2021a.** Turgor-limited predictions of tree growth, height and metabolic scaling over tree lifespans. *Tree Physiology* **42**: 229–252.

**Potkay A, Trugman AT, Wang Y, Venturas MD, Anderegg WR, Mattos CR, Fan Y. 2021b.** Coupled whole-tree optimality and xylem hydraulics explain dynamic biomass partitioning. *New Phytologist* **230**: 2226–2245.

**Poyatos R, Aguadé D, Galiano L, Mencuccini M, Martínez-Vilalta J. 2013.** Drought-induced defoliation and long periods of near-zero gas exchange play a key role in accentuating metabolic decline of Scots pine. *New Phytologist* **200**: 388–401.

**Poyatos R, Aguade D, Martínez-Vilalta J. 2018.** Below-ground hydraulic constraints during drought-induced decline in Scots pine. *Annals of Forest Science* **75**: 100.

**Preisler Y, Hölttä T, Grünzweig JM, Oz I, Tatarinov F, Ruehr NK, Rotenberg E, Yakir D. 2022.** The importance of tree internal water storage under drought conditions. *Tree Physiology* **42**: 771–783.

**Preisler Y, Tatarinov F, Grünzweig JM, Yakir D. 2021.** Seeking the "point of no return" in the sequence of events leading to mortality of mature trees. *Plant, Cell & Environment* **44**: 1315–1328.

**Prentice IC, Dong N, Gleason SM, Maire V, Wright IJ. 2014.** Balancing the costs of carbon gain and water transport: testing a new theoretical framework for plant functional ecology. *Ecology Letters* **17**: 82–91.

**Pretzsch H. 2014.** Canopy space filling and tree crown morphology in mixed species stands compared with monocultures. *Forest Ecology and Management* **327**: 251–264.

**Resco V, Ewers BE, Sun W, Huxman TE, Weltzin JF, Williams DG. 2009.** Drought-induced hydraulic limitations constrain leaf gas exchange recovery after precipitation pulses in the $C_3$ woody legume, *Prosopis velutina*. *New Phytologist* **181**: 672–682.

**Reyer CPO, Silveyra Gonzalez R, Dolos K, Hartig F, Hauf Y, Noack M, Lasch-Born P, Rötzer T, Pretzsch H, Meesenburg H *et al.* 2020.** The PROFOUND database for evaluating vegetation models and simulating climate impacts on European forests. *Earth System Science Data* **12**: 1295–1320.

**Rosas T, Mencuccini M, Barba J, Cochard H, Saura-Mas S, Martínez-Vilalta J. 2019.** Adjustments and coordination of hydraulic, leaf and stem traits along a water availability gradient. *New Phytologist* **223**: 632–646.

**Sabot ME, De Kauwe MG, Pitman AJ, Medlyn BE, Verhoef A, Ukkola AM, Abramowitz G. 2020.** Plant profit maximization improves predictions of European forest responses to drought. *New Phytologist* **226**: 1638–1655.

**Sala A, Woodruff DR, Meinzer FC. 2012.** Carbon dynamics in trees: feast or famine? *Tree Physiology* **32**: 764–775.

**Salmon Y, Lintunen A, Dayet A, Chan T, Dewar R, Vesala T, Hölttä T. 2020.** Leaf carbon and water status control stomatal and nonstomatal limitations of photosynthesis in trees. *New Phytologist* **226**: 690–703.

**Salomón RL, Limousin JM, Ourcival JM, Rodríguez-Calcerrada J, Steppe K. 2017.** Stem hydraulic capacitance decreases with drought stress: implications for modelling tree hydraulics in the Mediterranean oak *Quercus ilex*. *Plant, Cell & Environment* **40**: 1379–1391.

**Sapes G, Demaree P, Lekberg Y, Sala A. 2021.** Plant carbohydrate depletion impairs water relations and spreads via ectomycorrhizal networks. *New Phytologist* **229**: 3172–3183.

**Sapes G, Roskilly B, Dobrowski S, Maneta M, Anderegg WR, Martinez-Vilalta J, Sala A. 2019.** Plant water content integrates hydraulics and carbon depletion to predict drought-induced seedling mortality. *Tree Physiology* **39**: 1300–1312.

**Sapes G, Sala A. 2021.** Relative water content consistently predicts drought mortality risk in seedling populations with different morphology, physiology, and times to death. *Plant, Cell & Environment* **44**: 3322–3335.

**Schiestl-Aalto P, Kulmala L, Mäkinen H, Nikinmaa E, Mäkelä A. 2015.** CASSIA – a dynamic model for predicting intra-annual sink demand and interannual growth variation in Scots pine. *New Phytologist* **206**: 647–659.

**Schiestl-Aalto P, Ryhti K, Mäkelä A, Peltoniemi M, Bäck J, Kulmala L. 2019.** Analysis of the NSC storage dynamics in tree organs reveals the allocation to belowground symbionts in the framework of whole tree carbon balance. *Frontiers in Forests and Global Change* **2**: 17.

**Scoffoni C, Albuquerque C, Brodersen CR, Townes SV, John GP, Bartlett MK, Buckley TN, McElrone AJ, Sack L. 2017.** Outside-xylem vulnerability, not xylem embolism, controls leaf hydraulic decline during dehydration. *Plant Physiology* **173**: 1197–1210.

**Sevanto S, Hölttä T, Holbrook NM. 2011.** Effects of the hydraulic coupling between xylem and phloem on diurnal phloem diameter variation. *Plant, Cell & Environment* **34**: 690–703.

**Sevanto S, McDowell NG, Dickman LT, Pangle R, Pockman WT. 2014.** How do trees die? A test of the hydraulic failure and carbon starvation hypotheses. *Plant, Cell & Environment* **37**: 153–161.

**da Silva AP, Kay BD, Perfect E. 1994.** Characterization of the least limiting water range of soils. *Soil Science Society of America Journal* **58**: 1775–1781.

**Siqueira M, Katul G, Porporato A. 2009.** Soil moisture feedbacks on convection triggers: the role of soil–plant hydrodynamics. *Journal of Hydrometeorology* **10**: 96–112.

**Smith AM, Stitt M. 2007.** Coordination of carbon supply and plant growth. *Plant, Cell & Environment* **30**: 1126–1149.

**Smith DD, Sperry JS. 2014.** Coordination between water transport capacity, biomass growth, metabolic scaling and species stature in co-occurring shrub and tree species. *Plant, Cell & Environment* **37**: 2679–2690.

**Smith NG, Keenan TF, Colin Prentice I, Wang H, Wright IJ, Niinemets Ü, Crous KY, Domingues TF, Guerrieri R, Ishida FY *et al.* 2019.** Global photosynthetic capacity is optimized to the environment. *Ecology Letters* **22**: 506–517.

**Sperry JS, Adler FR, Campbell GS, Comstock JP. 1998.** Limitation of plant water use by rhizosphere and xylem conductance: results from a model. *Plant, Cell & Environment* **21**: 347–359.

**Sperry JS, Love DM. 2015.** What plant hydraulics can tell us about responses to climate-change droughts. *New Phytologist* **207**: 14–27.

**Sperry JS, Venturas MD, Anderegg WR, Mencuccini M, Mackay DS, Wang Y, Love DM. 2017.** Predicting stomatal responses to the environment from the optimization of photosynthetic gain and hydraulic cost. *Plant, Cell & Environment* **40**: 816–830.

**Sperry JS, Wang Y, Wolfe BT, Mackay DS, Anderegg WR, McDowell NG, Pockman WT. 2016.** Pragmatic hydraulic theory predicts stomatal responses to climatic water deficits. *New Phytologist* **212**: 577–589.

**Steppe K, De Pauw DJ, Lemeur R, Vanrolleghem PA. 2006.** A mathematical model linking tree sap flow dynamics to daily stem diameter fluctuations and radial stem growth. *Tree Physiology* **26**: 257–273.

**Thomas DS, Eamus D, Bell D. 1999.** Optimization theory of stomatal behaviour: II. Stomatal responses of several tree species of north Australia to changes in light, soil and atmospheric water content and temperature. *Journal of Experimental Botany* **50**: 393–400.

**Thompson MV, Holbrook NM. 2003a.** Application of a single-solute non-steady-state phloem model to the study of long-distance assimilate transport. *Journal of Theoretical Biology* **220**: 419–455.

**Thornley JHM. 1970.** Respiration, growth and maintenance in plants. *Nature* **227**: 304–305.

**Thornley JHM. 1971.** Energy, respiration, and growth in plants. *Annals of Botany* **35**: 721–728.

**Tomasella M, Petrussa E, Petruzzellis F, Nardini A, Casolo V. 2020.** The possible role of non-structural carbohydrates in the regulation of tree hydraulics. *International Journal of Molecular Sciences* **21**: 144.

**Torres LC, Keller T, de Lima RP, Tormena CA, de Lima HV, Giarola NFB. 2021.** Impacts of soil type and crop species on permanent wilting of plants. *Geoderma* **384**: 114798.

**Torres-Ruiz JM, Cochard H, Mencuccini M, Delzon S, Badel E. 2016.** Direct observation and modelling of embolism spread between xylem conduits: a case study in Scots pine. *Plant, Cell & Environment* **39**: 2774–2785.

**Trugman AT, Detto M, Bartlett MK, Medvigy D, Anderegg WRL, Schwalm C, Schaffer B, Pacala SW. 2018.** Tree carbon allocation explains forest drought-kill and recovery patterns. *Ecology Letters* **21**: 1552–1560.

**Urli M, Porté AJ, Cochard H, Guengant Y, Burlett R, Delzon S. 2013.** Xylem embolism threshold for catastrophic hydraulic failure in angiosperm trees. *Tree Physiology* **33**: 672–683.

**Valentine HT, Mäkelä A. 2012.** Modeling forest stand dynamics from optimal balances of carbon and nitrogen. *New Phytologist* **194**: 961–971.

**Van der Ent RJ, Savenije HHG. 2011.** Length and time scales of atmospheric moisture recycling. *Atmospheric Chemistry and Physics* **11**: 1853–1863.

**Venturas MD, Sperry JS, Love DM, Frehner EH, Allred MG, Wang Y, Anderegg WR. 2018.** A stomatal control model based on optimization of carbon gain versus hydraulic risk predicts aspen sapling responses to drought. *New Phytologist* **220**: 836–850.

**Venturas MD, Todd HN, Trugman AT, Anderegg WR. 2021.** Understanding and predicting forest mortality in the western United States using long-term forest inventory data and modeled hydraulic damage. *New Phytologist* **230**: 1896–1910.

**Von Allmen EI, Sperry JS, Smith DD, Savage VM, Enquist BJ, Reich PB, Bentley LP. 2012.** A species-level model for metabolic scaling of trees II. Testing in a ring- and diffuse-porous species. *Functional Ecology* **26**: 1066–1076.

**Wang Y, Sperry JS, Anderegg WR, Venturas MD, Trugman AT. 2020.** A theoretical and empirical assessment of stomatal optimization modeling. *New Phytologist* **227**: 311–325.

**Waring RH, Landsberg JJ, Williams M. 1998.** Net primary production of forests: a constant fraction of gross primary production? *Tree Physiology* **18**: 129–134.

**Wiley E, Helliker B. 2012.** A re-evaluation of carbon storage in trees lends greater support for carbon limitation to growth. *New Phytologist* **195**: 285–289.

**Witelski T, Bowen M. 2015.** Variational principles. In: *Methods of mathematical modelling*. Cham, Switzerland: Springer, 47–83.

**Wolf A, Anderegg WR, Pacala SW. 2016.** Optimal stomatal behavior with competition for water and risk of hydraulic impairment. *Proceedings of the National Academy of Sciences, USA* **113**: E7222–E7230.

**Xia J, Yuan W, Lienert S, Joos F, Ciais P, Viovy N, Wang Y, Wang X, Zhang H, Chen Y *et al.* 2019.** Global patterns in net primary production allocation regulated by environmental conditions and forest stand age: a model-data comparison. *Journal of Geophysical Research: Biogeosciences* **124**: 2039–2059.

**Zemp DC, Schleussner CF, Barbosa H, Rammig A. 2017.** Deforestation effects on Amazon forest resilience. *Geophysical Research Letters* **44**: 6182–6190.

**Zenes N, Kerr KL, Trugman AT, Anderegg WR. 2020.** Competition and drought alter optimal stomatal strategy in tree seedlings. *Frontiers in Plant Science* **11**: 478.

**Zha T, Kellomäki S, Wang KY, Ryyppö A, Niinistö S. 2004.** Seasonal and annual stem respiration of Scots pine trees under boreal conditions. *Annals of Botany* **94**: 889–896.

**Zhou S, Duursma RA, Medlyn BE, Kelly JW, Prentice IC. 2013.** How should we model plant responses to drought? An analysis of stomatal and non-stomatal responses to water stress. *Agricultural and Forest Meteorology* **182**: 204–214.

**Zweifel R, Sterck F, Braun S, Buchmann N, Eugster W, Gessler A, Häni M, Peters RL, Walthert L, Wilhelm M *et al.* 2021.** Why trees grow at night. *New Phytologist* **231**: 2174–2185.

## Supporting Information

Additional Supporting Information may be found online in the Supporting Information section at the end of the article.

**Fig. S1** Flowchart and comparison of model structures from growth optimization hypothesis and assimilation optimization hypotheses.

**Fig. S2** Steady-state growth optimization hypothesis responses of key model variables for potential values of stomatal conductance under varied environmental forcings.

**Fig. S3** Temperature dependence of the whole-stem extensibility.

**Fig. S4** Predictions of $R_{M,0}$ that satisfy NPP : GPP = 0.45 under steady-state growth optimization.

**Fig. S5** Predictions of $\widetilde{\phi}$ that satisfy NPP : GPP = 0.45 under steady-state growth optimization.

**Fig. S6** Predictions of NSC reserves ($C$) that satisfy NPP : GPP = 0.45 under steady-state growth optimization.

**Fig. S7** Percent change in nonstructural carbohydrate storage between elevated and ambient atmospheric $CO_2$ concentrations under steady-state growth optimization.

**Fig. S8** Sensitivity ($m$) of growth optimization hypothesis predicted stomatal conductance to vapor-pressure deficit.

**Fig. S9** Comparison of steady-state growth optimization hypothesis predictions to all of the considered assimilation optimization hypotheses.

**Fig. S10** Change in the marginal water-use efficiency between elevated and ambient atmospheric $CO_2$ concentrations under steady-state growth optimization.

**Fig. S11** Percent change in growth rate between elevated and ambient atmospheric $CO_2$ concentrations under steady-state growth optimization.

**Fig. S12** Change in stomatal conductance between elevated and ambient atmospheric $CO_2$ concentrations under steady-state growth optimization.

**Fig. S13** Change in the marginal water-use efficiency between elevated and ambient atmospheric $CO_2$ concentrations under steady-state growth optimization if trees adapted to elevated atmospheric $CO_2$ concentrations have acclimated their leaf traits.

**Fig. S14** Difference in growth rate between trees with and without acclimation of leaf traits, both of which grow under elevated atmospheric $CO_2$ concentrations.

**Fig. S15** Comparison of responses of growth optimization model to losses in hydraulic conductance following the two different approaches for the calculation of how stomata respond to conductance losses.

**Fig. S16** Comparison of predictions by growth optimization hypothesis and assimilation optimization hypothesis models under varied hydraulic conductance following the alternative approach of Venturas *et al.* (2018) to account for how permanent conductance losses impact predictions.

**Fig. S17** Phase diagram of nonstructural carbohydrate and percent loss of conductance resulting from acclimation to permanent water stress or from postdrought recovery after transient water stress following the alternative approach of Venturas *et al.* (2018) to account for how permanent conductance losses impact predictions.

**Notes S1** Full model, parameter estimation, and simulation descriptions.

**Notes S2** MATLAB code for model and plotting/analyzing data, including forcing data and simulation outputs.

**Table S1** Main variables and symbols in model.

**Table S2** Additional stomatal optimization models and studies testing their predictions.

Please note: Wiley is not responsible for the content or functionality of any Supporting Information supplied by the authors. Any queries (other than missing material) should be directed to the *New Phytologist* Central Office.